ÉCOLE CENTRALE DE NANTES FIRST YEAR INSTITUTION

MASTER ARIA-ROBA

"AUTOMATIQUE, ROBOTIQUE ET INFORMATIQUE APPLIQUÉE"

2016 / 2017

Master Thesis Report

Presented by

Matthieu Furet

21/07/2017

Design and control of exploration robot with reduced energy consumption

Jury

President:	Philippe Martinet	Professor (ECN-LS2N)
	Olivier Kermorgant	Professor (ECN-LS2N)
Evaluators:	Ina Taralova	Professor (ECN-LS2N)
	Philippe Martinet	Professor (ECN-LS2N)
	Olivier Kermorgant	Professor (ECN-LS2N)
	Sebastien Briot	CNRS researcher (LS2N)
	Rafael Balderas Hill	PhD student (LS2N)
Supervisor(s):	Sebastien Briot	CNRS researcher (LS2N)
	Rafael Balderas Hill	PhD student (LS2N)

Laboratory: Laboratoire des Sciences du Numérique de Nantes LS2N

Abstract

Exploration robots are used for numerous applications, from space exploration to unstructured environment such as cities destroyed by earthquake, nuclear plants for security surveillance, forest for fire surveillance... One of the main problems of exploration robots is their lack of autonomy. In fact, if a robot needs to be more energetically autonomous, it needs more batteries and additional electrical components, leading to a heavier robot. And a heavier robot needs more power and more energy to move itself. To go out of this vicious circle, one needs to find ways to reduce the energy consumption of the robot. One fashioned way to reduce energy consumption of robots is to use variable stiffness actuators (VSA), which can adapt their stiffness to the task in order to have the most energy efficient motion. If a mobile robot must move following a periodic motion, the use of VSA in order to put the system in resonance is possible, and would considerably reduce the energy consumption. In this master thesis, we will try to prove that VSA can help to reduce energy consumption of a system, by designing a mobile robot and compare its energy consumption for a nominal case, a case with fixed stiffness springs and VSA, based on a computation of the losses of the full actuation chain (electrical and mechanical losses).

Acknowledgments

Before starting this master thesis report, I would like to thank the people who helped me during this last six months, and the jury of the master thesis for their attention.

First, I would like to thank my supervisor **Sebastien Briot** for his precious help and advice during the thesis. We knew how to encourage me and keep a fluent development of the research work even when the results did not came as fast a I thought. It was a pleasure and a very rewarding experience to work with him, I learned a lot about the world of research thanks to his experience.

I would also thank **Rafael Balderas Hill**, my other supervisor and PhD student, for his huge support along the thesis. I really appreciated to work with him, and as a supervisor for the first time he did an outstanding work. Thank you for the time you gave to me and to correct my wobbly English

Finally, I would like to thank the PhD students of the **ARMEN team** and all the Master thesis students who answered my specific questions, and of course all the teachers and researchers of the **ARIA-ROBA master**.

Contents

List of Figures

List of symbols

m : Weight of one mass
R : Radius of the cylinder
J_{ds} : Inertia of the cylinder
J_{sc} : Inertia of the screw
p : Reduced ratio of the ball screw
q_i : Angular position of the i-th actuator
r_i : Position of the i-th mass on the ball-screw
θ : Angular position of the sphere
d : longitudinal position of the center of the cylinder
$\mathbf{q}$: Vector of generalized coordinates
$\mathbf{M}$: Inertia Matrix
$\mathbf{h}$: Function of gravity, centrifugal and Coriolis effects
τ_i : Input torque of the i-th actuator
$\boldsymbol{\tau}_L$: Vector of mechanical torques on the actuators
L : Lagrangian of the system
T : Kinetic energy of the system
V : Potential energy of the system

F_n : Normal friction force
F_t : Tangential friction force
μ : Friction coefficient
v_s : Stiction transition velocity
v_d : Friction transition velocity
μ_s : Static coefficient of friction
μ_d : Dynamic coefficient of friction

$\mathbf{q}_{des}$: Desired trajectory of the masses
$\mathbf{q}_{feed}$: Feedback of the mass trajectories

v : Error vector

$\mathbf{K}_p$: Matrix of proportional gain

$\mathbf{K}_d$: Matrix of derivative gain

$\boldsymbol{\tau}_e$: Vector of electromagnetic torques

P_{losses} : Power of the electrical and mechanical losses

$\boldsymbol{\alpha}$: Matrix of optimization variables

$\mathbf{K}$: Stiffness matrix

$\mathbf{q}_s$: Vector of angular positions of VSAs

J_{vsa} : Inertia of the VSA

Chapter 1

Introduction and Aim of the thesis

Discovery and exploration always took a big place in mankind history. Today, almost everything reachable has been explored. New tools are necessary to explore space, seabed... Tools are also needed to explore fields where the human is not welcomed: Destroyed cities, nuclear plants, mine fields,etc. Robots can answer to this problems. They dispose of enough capabilities to explore unstructured environment, thanks to motors, sensors, control commands. There are several types of exploration robots, from rolling and tracked robot to humanoid robots, and each kind of robot has its own predilection field. Our purpose will be to make a state of the art of mobile robots and highlights some technologies that might be interesting for this master thesis.

Every robot needs a power source to move itself. For a fixed robot in factory, they are connected to the electric network. However an exploration robot has to be autonomous, so it has to carry its own source of energy. For most of them, the main form of energy used is electric energy stored in batteries. In some applications, robots can reload their batteries from an external power source, like solar energy for space exploration robots. But if not, robot have to carry all the energy they need. So the more they consume, the more batteries they need. And as a heavier robot needs more energy to move itself, the research on energy efficiency is a necessity. For exploration robots, this energy efficiency can be improved in a lot of different ways. The first approach is of course to try to reduce the mass of robots, by optimizing materials and building on the robot. This is a static optimization. Another way is to optimize the path planning, with the first following assumption : the shortest path is not always the most energy efficient one. At last, one can also try to optimize the actuators to reduce energy, as they are the parts of robots that consume electric energy when they work as a generator. This is the dynamic optimization.

As said right before, an interesting way to reduce energy consumption is to focus on the actuators used in exploration robots. Classical electric motors are cheap, have a good efficiency and are easy to control. However they have a limited dynamic behavior and Today, they are a restriction for the robotic growth. Humans and animals are always adapting the stiffness and damping of their limbs unconsciously, in order to have the best rebound and to have the most efficient motion. For more than ten years, researchers are trying to reproduce this behavior with compliant joints, combining a classical motor with a compliant element such as a spring. At first, the spring had a fixed stiffness chosen to optimize the task at a certain speed, but now with Variable stiffness actuators (VSA), the stiffness is tuned with a mechanic chain or some other physical principle. They have several advantages, as making the robot more adaptable to different environments in order to safely interact with humans and to have a more energy efficient functioning by storing and releasing energy in the passive elastic elements.

The aim of the master thesis is to design and model an exploration robot with reduced energy consumption, by using compliant elements. The requirements have been defined in the end of the bibliography work, for example : The kind of mobile robot we will use, the technology for the variable stiffness actuators, the control law, etc.

Chapter 2

Bibliography work

2.1. State of the art of mobile robots

2.1.1 Introduction

As said before, mobile robots are used for several applications such as space exploration, nuclear plant investigation, demining [20], and on diverse fields like flat ground, mountains, forest, etc. That is why the diversity of technologies for this kind of robot is huge and hard to refer. In order to have a quite exhaustive state of the art, several reviews which deal with several technologies for a same type of mobile robot are considered. According to [4], most of mobile robots can be classified into 5 categories :

- Wheeled robots
- Tracked robots
- «Snake» robots
- Legged robots
- Wheel-legged robots

In this report, the state of the art will be detailed, according to this classification but with some modifications : The first subsection will deal with both wheeled and tracked robots, as they will rapidly be put out of the study. The second subsection will be about rolling robots, which are robots rolling on their entire outer surface [2]. The third subsection will group the legged robots, in which the most well-known and

represented platforms are the humanoid robots. The next part deals with the Wheeled-leg robots or ≪Whegs≫ robots [21], which would be interesting for our subject. The last subsection is about crawling and tensegrity robots which have really emerged in the last few years.

2.1.2 Wheeled and tracked robots

In this subsection, only small wheeled robots designed for exploration or simple tasks are taken into account. Autonomous cars and vehicles are considered out of the study. Wheeled and tracked robots are mainly used in humanitarian demining [20], as it is a very dangerous task for a human, and the field is mainly flat and attainable for a wheeled robot. Some of them are not really robots but can be considered as drones because they are commanded by distance.

Tracked robots are also used for exploration for their good capacities of exploration on various fields. In fact, they are more adequate to explore all kind of terrains than wheeled robots, and they are used a lot for demining (figure 2.1) [20].

Figure 2.1: Tracked demining robot [1]

Wheeled and tracked robots are very robust, easy to design and to command. They are used a lot for simple exploration tasks but very limited in some environments. For this kind of robots, the torque applied on the motors is often continuous and not periodic, so they will not be very useful for our subject.

2.1.3 Rolling robots

A rolling robot is a robot which rolls on its entire outer surface. Thus they tend to be spherical or cylindrical. They have a lot of advantages over other kind of robots [2]:

- The entire robot system is put inside the spherical shape and thus provides mechanical and sometimes even environmental protection to equipment and components.

- There are no extremities that can hang-upon obstacles like sticks or rocks.
- The entire outer body rotates helping the device to cover uneven or soft surfaces.
- Spherical robots have no «edge» to fall over upon from which would be stuck.
- They can be used for traveling on soft grounds such as sand, snow, brush, or vegetation.
- Rolling spheres can potentially move in any direction and turn when meeting objects they cannot pass. This makes their control relatively easy.

All the rolling robots presented next are based on the principle of moving the center of gravity outside the contact area, which causes the sphere to move in this direction (figure 2.2).

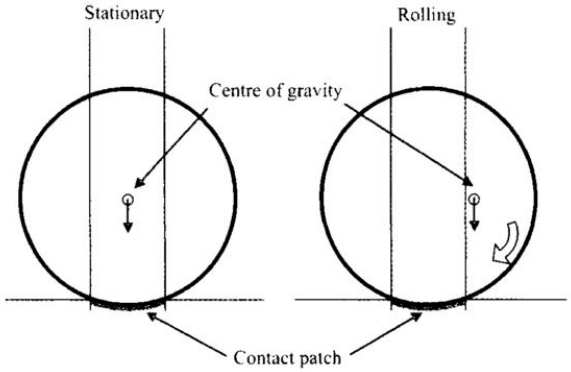

Figure 2.2: Rolling by moving center of gravity [2]

There are numerous systems for rolling robots, but one can distinguish seven main technologies : sprung central axis, car driven, mobile masses, spherical wheels, gyroscopic stabilization, ballast mass on a fixed axis and ballast mass on a moving axis. Some of them will not be presented in much detail because there are few real applications and they would not be very useful for our subject.

One drawback for this kind of robot is the fact that they need their entire outer surface to move. So this surface cannot be used for other tasks, like a place for sensors or information device. The rolling robots are often designed with a retractable camera to position themselves in the environment, or with GPS devices.

Mobile masses

The third concept uses the movement of masses along several radial axis of the sphere. This design allows motions in every direction at any time, because the position of the

center of the sphere can be changed very quickly (figure 2.3). The motion is quite difficult to command because all the masses have to be controlled simultaneously. One robot using mobile masses has been prototyped, the August robot (figure 2.4). The propulsion mechanism consists of four powered spoke screw, connected in 109.47°, inside a tetrahedral shape.

This kind of robot can be very interesting for our study. Indeed, the motion of mobile masses, in order to have a straight line with constant speed displacement, will be periodic and quite fast. So the use of variable stiffness actuators and the resonance of the system can be a good idea to reduce the energy consumption of such robot.

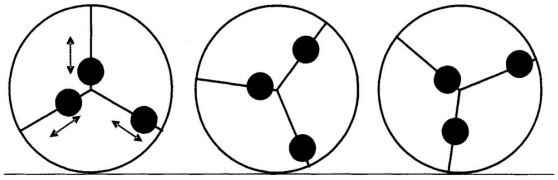

Figure 2.3: Principle of mobile masses [2]

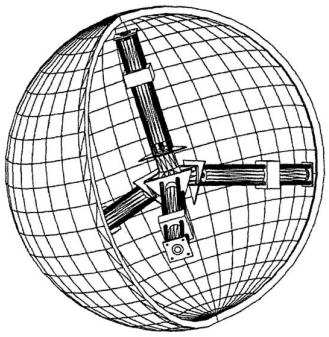

Figure 2.4: CAD of the August robot [3]

2.1.4 Legged robots

Most of animals are using legs, because this solution permits to adapt to numerous fields like mountain land, forest, sand, and rugged terrain with various obstacle. Therefore, they are more difficult to control and sometimes more energy consuming. This report focuses on three big classes of legged robots : Heavy-duty legged robots, quadruped and biped robots.

The interesting aspect of this review is to compare all the designs used for legs. In fact, there are many mechanical structures and all of them have a huge impact on the behavior of the robot and the energy consumption (figure 2.5). Many other aspects need

to be taken into account like arrangement of legs, number of legs, number of driving joints [22].

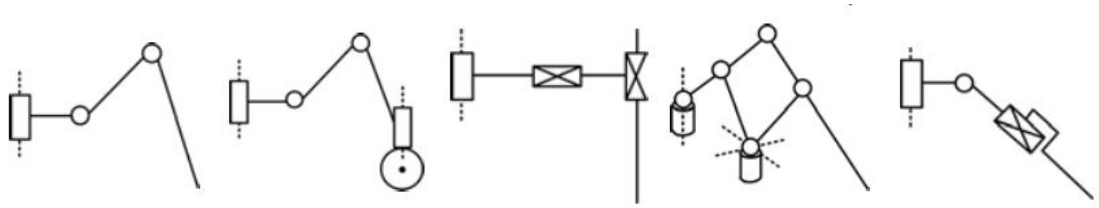

Figure 2.5: Mechanical structures of legs, from left to right : articulated leg type 1 and type 2, Cartesian Coordinate leg, Pantograph leg and Telescopic leg [4]

2.1.5 «Whegs» robots

Whegs robots are robots which use wheel-legs to move [21]. Inspired by the motion of the cockroach, they are very efficient on fields with obstacles, as their legs permits them to cross obstacles and move on various type of fields. They can also be interesting for our subject because for a simple motion, the torque is not constant as it could be for a simple wheeled robot. The dynamics are quite fast so compliant actuators could be used. Compliant actuators have been already used for whegs robots, for instance in the DAGSI Whegs [5]. In this case, the compliant joint is located between the two parts of the chassis (figure 2.6) and is here to absorb shocks (figure 2.7).

Figure 2.6: The DAGSI Whegs prototype [5]

2.1.6 Tensegrity robots

Tensegrity is an abbreviation for tensile integrity. A tensegrity system is established when a set of discontinuous compressive components interacts with a set of continuous

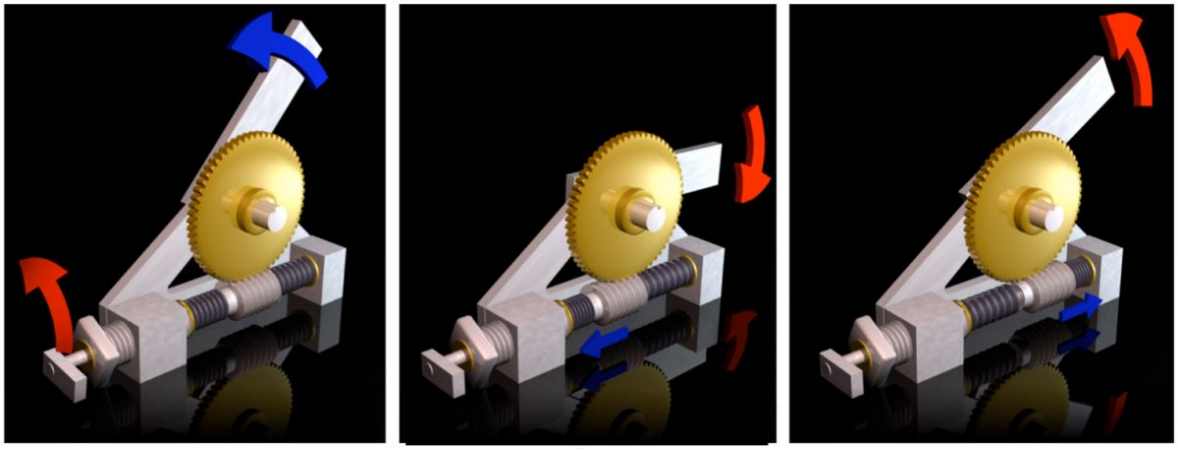

Figure 2.7: The compliant body joint of the DAGSI : When the worm is driven (red arrow on the left), the joint moves as a standard worm gear. But when an effort is applied on the joint (red arrow in the middle and the left), the worms moves axially and cushion the chock with bellville springs (blue arrows) [5]

tensile components to define a stable volume in space. Tensegrity robots are a quite new kind of system with a lot of applications, from art to robotics.

A tensegrity robot is composed by a set of rigid and soft components which are interconnected. The mechanism is lying on its outer surface and have several equilibrium position. To switch from one position to another, an actuator applies a deforming force at one point off the structure, moving the center of gravity of the system, like in the rolling robots.

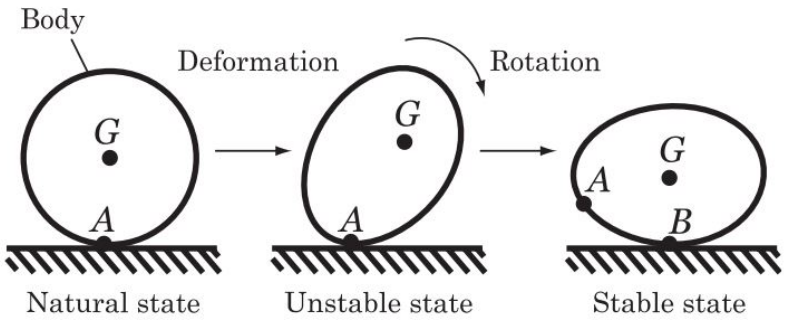

Figure 2.8: Principle of crawling by body deformation [6]

Tensegrity robots are strong and lightweight, easy to control. They have many advantages for space exploration, because they are lightweight and able to absorb shocks, so the landing is easier [23]. For our purpose, this technology can be interesting because it implies rigid and soft parts. To follow the general thinking, some variable compliance on the soft part can be added, in order to tune the stiffness of the links and have a

resonance of the system at a defined speed of exploration. Nevertheless, this kind of robot has very low dynamics, as they are traveling at low speeds, and it would also need to model the impact. Thus, it would be difficult to reduce energy consumption using resonance for this kind of robot.

2.1.7 Conclusion

This state of the art of mobile robotics detailed several types of mobile robots, and each type uses different technologies. As the subject is made, there is not so many constraints on the type of mobile robot to use. Indeed, the speed of exploration, the kind of field to explore are not defined. Thus, the most efficient technology to answer the main problem can be chosen : how to minimize the energy consumption.

Talking about energy consumption and high-efficiency, some solutions are out of the list. The use of compliant joints also add some constraints on the type of robots, as the wheeled robots which are out of our study. Indeed, the focus is more on robots where a periodicity in the efforts on the actuators can be found, such as legged robots, whegs or tensegrity robots.

As a first conclusion, some kind of rolling robots can also present this kind of periodicity, and this direction will be investigated during the master thesis.

2.2. Strategies for energy efficiency

2.2.1 Introduction

There are several criteria to define the performance of a system (accuracy, speed, torque, power,...). The one of research interest for this study is the energy efficiency. Usually, the efficiency of a system is defined as follows :

$$Efficiency = \frac{Output}{Input} \tag{2.1}$$

This is the criteria to maximize in this master thesis : To have the best quantity of output energy for an input energy. In mobile robotics, there are different tasks to achieve, but for our purpose of exploration, the task is to go from a point A to a point B with a certain speed.

The energy consumed by a system on a period T can be defined for a moving system by the following formula :

$$J = \int_0^T (V(t)F(t) + \omega(t)\Gamma(t))dt \tag{2.2}$$

with $V(t)$ the linear speed of the system, $F(t)$ the sum of the forces applied on the system, $\omega(t)$ the rotational velocity and $\Gamma(t)$ the torque applied on the system.

For instance, a robot with rotational actuators (such as DC motors), with a given velocity, the torque applied by the actuators needs to be reduced.

The efficiency can be improved statically and dynamically. On a static plan, the energy efficiency is obtained by optimal design and distribution of mass, balancing... A good example of energy based design on a static point of view can be found in [24].

This report focuses on the dynamic aspects of energy efficiency, which can be made by different approaches, such as the research of an optimized path, the numbers of actuators used, the use of compliant joints. This list is not exhaustive but the main approaches will be explained.

2.2.2 Trajectory planning

An exploration robot follows the instructions of a motion plan, which includes a path plan and a velocity schedule. The path plan specifies the trajectory of the robot whereas the velocity schedule specifies the changing in velocities, the accelerations and decelerations of the robot along its path.

For instance, if a robot has to explore several places, the route can be set to reduce the total distance, or to have the smoothest trajectory, without big turns and accelerations, or even to follow the path with the less of hills and bumps.

Mei et al. [7] tried to show the differences of efficiency regarding the strategy of exploration for a given area. They used an omnidirectional robot, following different path (figure 2.9).

They simulated the energy efficiency in m^2/J regarding the size of the area (figure 2.10). These results were validated with real experiments. For a small area, the scan lines are better because the robot has to do only a straight line to explore the area. But for a wider area, the spiral strategy is better because the robot does not have sharp turns so its avoiding big accelerations and decelerations. In the same way, the square spiral is better than the scan lines because it has less turns.

They also show that the energy efficiency is also affected by the velocity, but not as the first thinking : For low speeds, the robots consume more, but at a certain speed, the efficiency decreases.

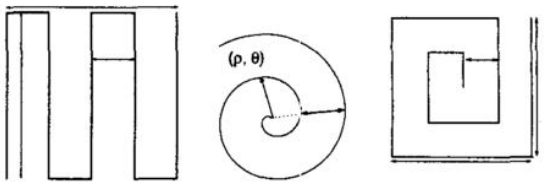

Figure 2.9: Different strategies of exploration : scan lines, spiral, square spiral [7]

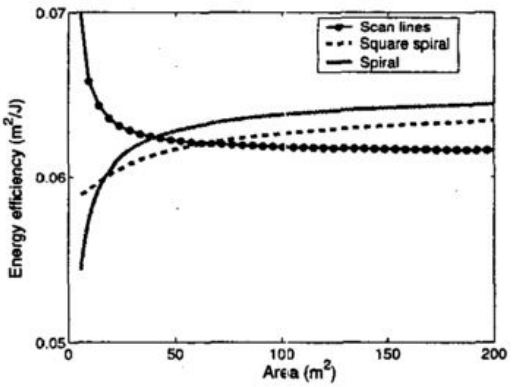

Figure 2.10: Energy efficiency of the different strategies of exploration [7]

2.2.3 Number of actuators, use of redundancy

The energy consumption of a system mainly comes from the actuators, because they generate the mechanical power needed for the system to move. To reduce energy consumption, one can try to optimize the actuators efficiency. Nowadays, very efficient motors already exist, like DC motors, and if it's easy and cheap to get from a 60% efficiency to a 80%, it is way more expensive to get from 80% to 95%. One have to search in other fields to improve energy efficiency, and one field which might be contradictory is the redundancy of the system. In fact, if the system has more actuators than needed, one might think that the system will consumes more energy.

The first researchers who worked on actuation redundancy are Pierrot and Company [25]. Their research in 2001 has shown that for a 3 DoF parallel robot with 4 actuators, redundancy allows the system to have a more lightweight structure, increasing the dynamic performances, and to a certain extend the energy consumption.

On an energy plan, [8] shows that energy consumption can be reduced thanks to a smart use of redundant actuation. These results are obtained for a parallel mechanism (figure 2.11) derived from an industrial manipulator (ABB IRB1410).

They establish the kinematic and dynamic model of the robot and choose a power consumption model considering the mechanical power output and the electrical power

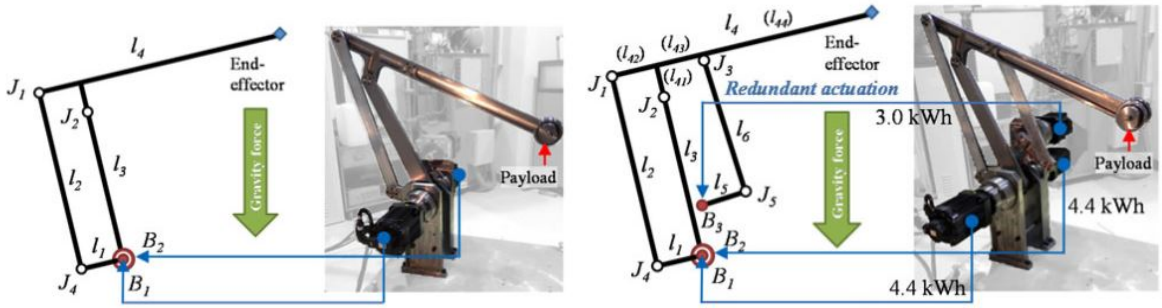

Figure 2.11: The full-actuated parallel mechanism on the left, and the over-actuated one on the right [8]

lost for classical servo-motors (heat in the coil, conduction in servo amplifiers and switching in servo drives), all depending on the current :

$$P_{total} = P_{output} + P_{loss} = \sum_{i=1}^{n} [\tau_i \dot{q_i}]^+ + \sum_{i=1}^{n} (\kappa_i^a |\tau_i| + \kappa_i^b \tau_i^2) \tag{2.3}$$

with n the number of actuators, τ_i and $\dot{q_i}$ the torque and angular velocity of actuator i, κ_i^a and κ_i^b coefficient of the power loss.

They made then several simulations and experimentations for a spot welding process of duration 78 s, with a payload of 10 kg. The two systems with and without redundant actuation are operating with the same velocities and the results are shown on figure 2.12. The non-redundant system is consuming way more power than the redundant one for a same task. The power consumption of the redundant system varies between the two strategies chosen : the classic strategy minimizing the energy cost, and the other with a different function cost, trying to reduce the sum of the torques on the actuators. The differences between simulation and experimentation are due to the friction in the joints and the gearbox.

This result can be useful for some kind of exploration robot. For example, a rolling robot based on the mobile masses technology can be designed with a reduced number of mobile masses (4 usually), but with this result, a design with more masses could be investigated.

2.2.4 Use of compliant joints

A lot of recent research in robotics have shown that using compliant joints such as serial elastic actuators (SEA) or variable stiffness actuators (VSA) can significantly improve safety and performance of systems. The first use of compliant joints were made on humanoid robotics to mimic the human musculo-skeletal system behavior. The first

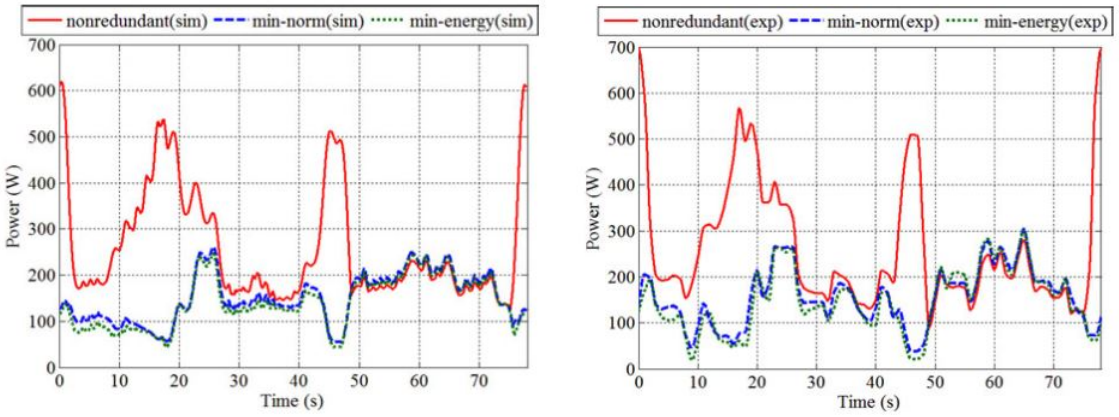

Figure 2.12: Graphs comparing the results without redundant actuation and with two strategies of redundant actuation. Simulation is on the left and experimentation on the right [8]

system were only made with a serial spring in the chain between the load and the actuator. More recent studies show the impact of VSA on the performance of the tasks.

[9] has shown that in a simple system, an optimal linear spring exists for a given inertia and motor. They has also shown that with an optimal control of a VSA, varying the stiffness during a task can improve the final performance.

The system used was a 1 DoF actuator doing a hammering task (figure 2.13). The simplest model of a compliant link, according to the scheme is the following (with $\omega = \sqrt{k/m}$) :

$$\ddot{q} + \omega^2(q - \theta) = 0 \tag{2.4}$$

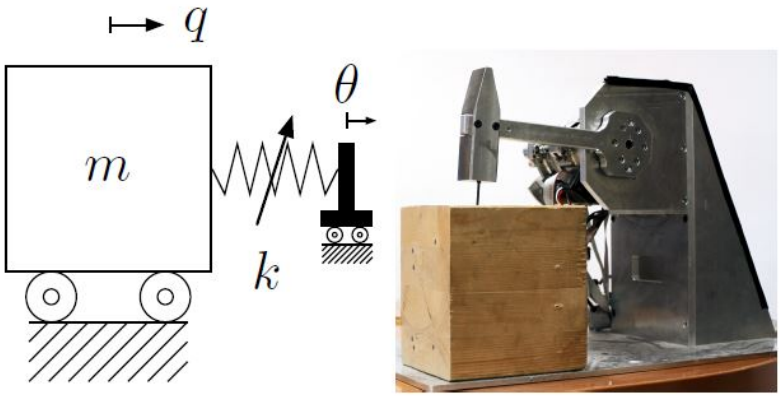

Figure 2.13: Scheme of the compliant actuator and the left and picture of the experimental device on the right [9]

The goal was here to maximize the link speed at the impact. They first investigated the speed optimization with Serial Elastic Actuator (SEA), with three different input control variables : position (P), speed (S) and acceleration (A). The results on figure 2.14 shows that the final link speed is directly linked to the stiffness k of the device, and that an optimal stiffness can be find to maximize the performance of the hammer.

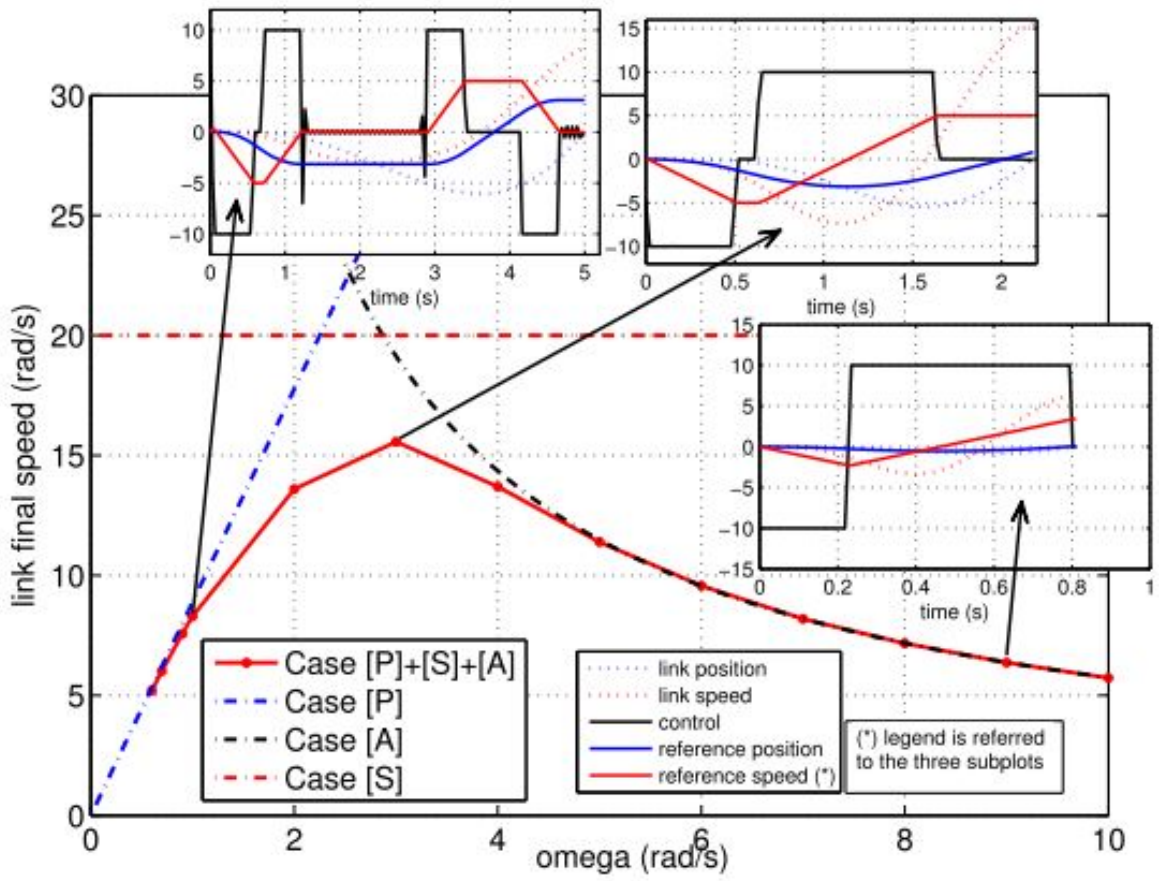

Figure 2.14: Maximal speed $\dot{\theta}$ and hit time for the different control variables, depending on ω. The red continuous link is case (A) with constraints on θ_{max} and $\dot{\theta}_{max}$ [9]

They then investigated the VSA problem with stiffness k and equilibrium position θ as inputs of the system. With an optimal control, detailed in [9], they conclude with a relation between the final speed that can be obtained with VSA and SEA :

$$\frac{v_{VSA}}{v_{SEA}} = \frac{1 + \sqrt{k_{max}/k_{min}}}{2} \tag{2.5}$$

with k_{max} and k_{min} the range of possible stiffness for the VSA. So (2.5) shows that we always have $V_{VSA} > V_{SEA}$. So Garabini et al. has shown that the use of VSA improves the performance of a system. The next subsection deals with the improvement of energy consumption thanks to VSA.

2.2.5 Resonance of a periodic system

The principle of resonance of a periodic system is based on the conventional resonance of a simple system, like a pendulum. This concept can then be generalized for multi-DoF systems. This section will detail the method of resonance, the applications and advantages. It will also compare several architecture for resonance (serial and parallel spring) and conclude on the improve of the performances.

Conventional resonance

The dynamic model for a 1 DoF system is :

$$m\ddot{q} + d\dot{q} + kq = \tau \tag{2.6}$$

with $q = a\sin(\omega t)$, and m, d and k respectively mass, viscosity and stiffness of the system. The theory of conventional resonance gives $k_{opt} = m\omega^2$, the stiffness minimizing the torque for the given sinusoidal motion. This concept can be generalized and extended for more complex robots with non-sinusoidal motion [10].

Resonance based control for multi DoF robots

For some years, researchers are trying to implement the conventional resonance in multi-DoF robotic systems, in order to have torque reduction and high energy efficiency. The idea is to put adjustable elastic elements between each joint of the robot (figure 2.15). This compliant element can be a simple spring with an adjustable stiffness, or the actuator and the compliant elements can be combined to form a variable stiffness actuator.

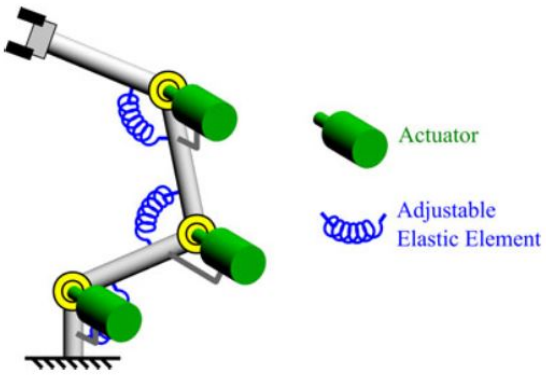

Figure 2.15: Serial robot with compliant elements on each joint [10]

Uemura et al. [10] applied this method to a SCARA robot for pick and place tasks (figure 2.16). The dynamic model of a SCARA robot can be written as follow :

$$\mathbf{R}(\mathbf{q})\ddot{\mathbf{q}} + \mathbf{h}(\mathbf{q}, \dot{\mathbf{q}}) + \mathbf{D}\dot{\mathbf{q}} = -\mathbf{K}(\mathbf{q} - \mathbf{q_e}) + \boldsymbol{\tau} \tag{2.7}$$

where $\mathbf{q}$ is the vector of joint angles, $\mathbf{q_e}$ the equilibrium position, $\mathbf{R}(\mathbf{q})$ an inertia matrix, $\mathbf{h}(\mathbf{q}, \dot{\mathbf{q}})$ the Coriolis vector, $\mathbf{D}$ and $\mathbf{K}$ respectively viscosity and stiffness diagonal matrices. $\boldsymbol{\tau}$ is the vector of control torque [26]. The control objective is to follow a desired trajectory, while minimizing the actuator torque vector $\boldsymbol{\tau}$ by optimizing the stiffness $\mathbf{K}$. The cost function was defined :

$$\mathbf{J}(\mathbf{K}) = \int_0^T \boldsymbol{\tau}^\top \mathbf{F} \boldsymbol{\tau} dt \tag{2.8}$$

with $\mathbf{F}$ a weighting diagonal matrix. So the optimal stiffness $\mathbf{K}_{opt}$ is given by $\mathbf{J}(\mathbf{K}_{opt}) = min_K \mathbf{J}(\mathbf{K})$.

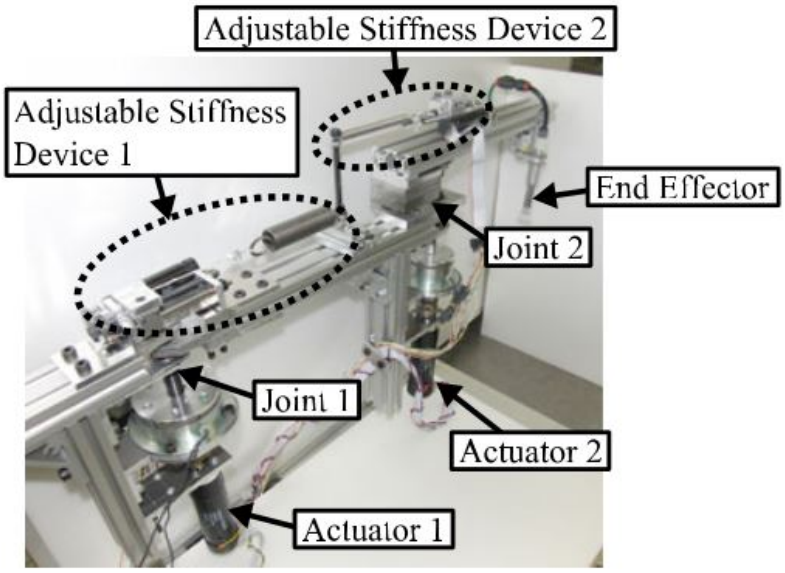

Figure 2.16: The modified SCARA robot with its compliant joints [10]

The motion is first obtained thanks to a feedback controller (not detailed here), which guarantees the convergence of the motion and the torque without requiring the exact knowledge of parameters values. But this control method needs high feedback gains which can cause high-frequency oscillation with a real system, so the team decided to implement a repetitive controller with feedforward input based on iterative learning control.

The results demonstrated that the method first reduces the actuator torques but also increases the accuracy of the system. The variable stiffness system consumes energy on

the beginning of the motion, to tune itself to the optimal stiffness, but then it consumes almost no energy. This assumption still has to be investigated, in order to see if the energy efficiency is really augmented.

Comparison between Series elastic actuators and Parallel elastic actuators

Several solutions are possible to design a compliant joint. Some of these solutions, in particular for variable stiffness actuators will be developed in the next chapter, but the main question is about the place of the compliant part regarding the rest of the system (the actuator, the ground, the load). [11] compared three cases for a rotational 1 DoF actuated pendulum : The case of the pendulum without compliant element (rigid actuator), a parallel elastic actuator (PEA) and a serial elastic actuator (SEA) (figure 2.17). The experiments have shown one more time the high efficiency of compliant system regarding the rigid one, but one step after by comparing to compliant system.

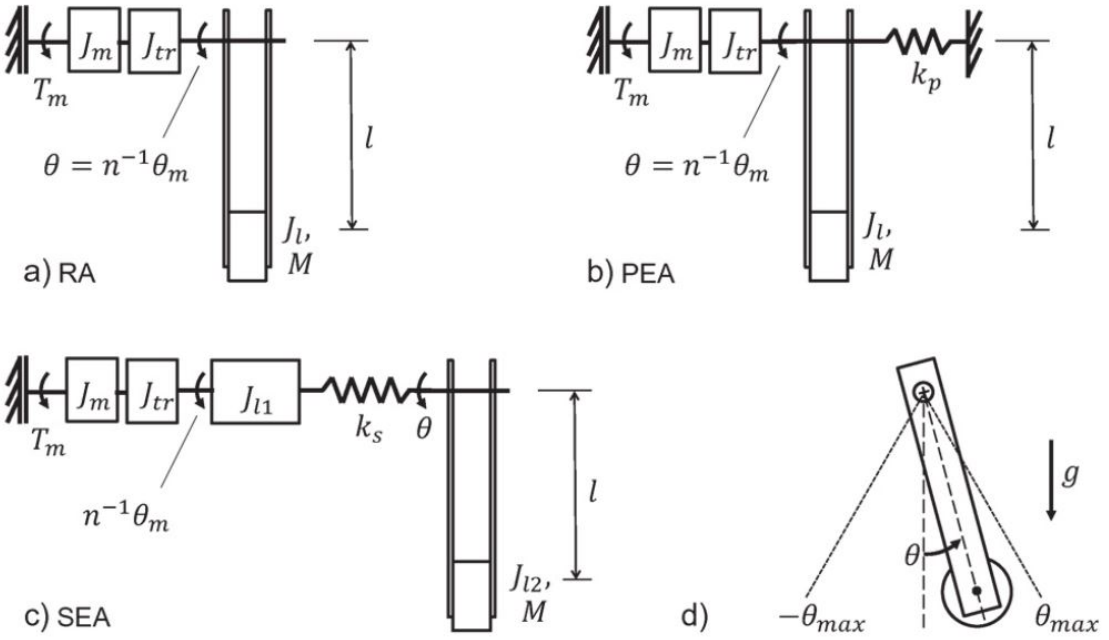

Figure 2.17: The three different pendulum technologies, with a front view in (d) [11]

The dynamic model of each pendulum is computed (not detailed here), and several remarkable frequencies are obtained. For the rigid system, the resonance frequency $\omega_{rs,RA}$ and the subsystem one $\omega_{rl,RA}$ are obtained. Idem for the PEA with $\omega_{rs,PEA}$ and $\omega_{rl,PEA}$ respectively. The equation motion of the SEA are more sophisticated and introduce several resonance frequencies : two resonance frequencies due to a fourth-order transfer function $\omega_{r1,SEA}$ and $\omega_{r2,SEA}$ and one anti-resonance frequency $\omega_{a,SEA}$.

The model of motor used to compute the power and energy consumption was a DC motor. Several graphs are obtained comparing the power and energy consumption, but the most interesting one is in figure 2.18. The black lines show the domain where the rigid system and the SEA (respectively PEA) works equally-well (relative energy difference is null). But the blue zone shows where the SEA and PEA systems are consuming less than the rigid system. The zones are delimited by the remarkable frequencies of the system, and this graphs shows that energy can be saved using compliant joints. The SEA seems to have a larger region where the gain of energy is important, thanks to a more favorable dynamic.

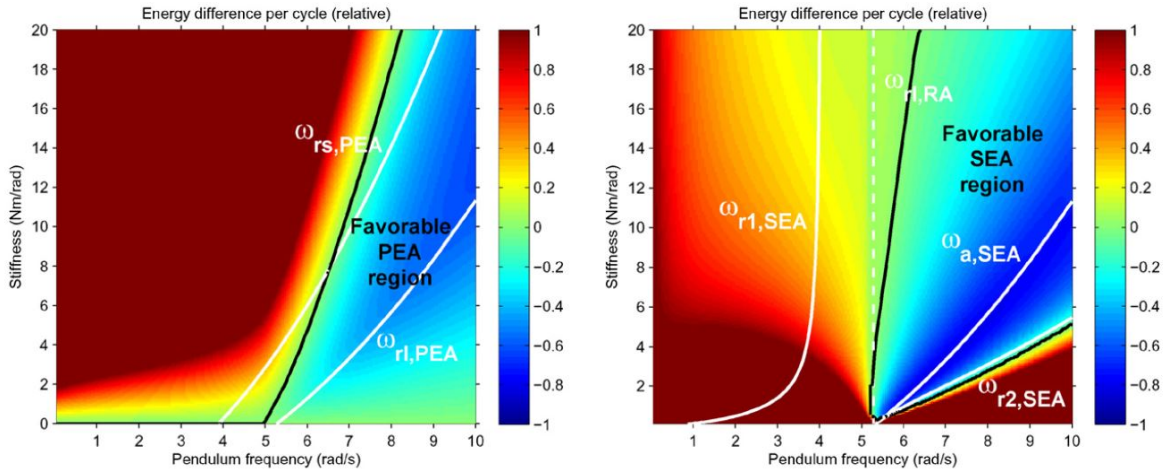

Figure 2.18: Energy difference between RA-PEA on the left and RA-SEA on the right, regarding the stiffness and the pendulum frequency [11]

2.2.6 Conclusion

This chapter dealt with the different strategies to optimize energy. They are numerous and some of them can be seen as conflicting, such as the redundancy of actuators in a system. The main strategy studied was the resonance-based strategy, because it involves compliant elements, which becomes very interesting in robotics. In fact, they have been used in several domains such as humanoid robotics, pick-and-place tasks and exo-skeleton, and more research has to be done to integrate them in other kind of robots. The aim of the master thesis would be to design an innovative mobile robot using the strategy of resonance to reduce its energy consumption. Some previous studies have shown that using compliant element is already increasing energy efficiency, some others that a variable stiffness element is better. The state of the art of VSA is huge, there is a lot of different concepts and technologies, and the choice of a VSA for an exploration

robot requires to explore this field.

2.3. State of the art of Variable Stiffness Actuators

2.3.1 Definition and Classification

An actuator is the central element of a system, which provides power and allows the system to move. It is characterized by two quantities, the flow quantity (the velocity or angular velocity) and the potential quantity (force or moment) depending if the actuator is a linear or angular one. These two quantities are linked thanks to the load, which can be seen as an impedance in a frequency approach.

A classic actuator can be controlled only on one of this quantity, and the impedance between the two is infinite (theoretically). That means that for an actuator controlled by a speed law, when this actuator comes to be blocked, there is no possible deviation for it. The first compliant actuators were developed in humanoid robotics, giving a possible deviation of the joint around its equilibrium position. They are called serial elastic actuator (SEA). This first compliant joints were made with a spring or a damper with a fixed impedance.

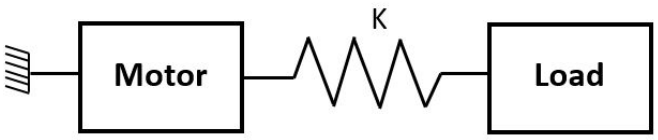

Figure 2.19: Series elastic actuator schematic

On the contrary, a variable impedance actuator is able to change the relation between the flow quantity and effort quantity. In other words, the impedance is no more infinite nor fixed and can be changed, regarding the task.

A mechanic impedance depends on several quantities : mass, inertia, damping, stiffness... All these quantities offer many possibilities to design a variable impedance actuator. The different technologies based on [13] are detailed on table 2.1. There is two main categories, one where the impedance is seen as a coupling between damping and stiffness, and one where only stiffness can be modified. This last category contains the Variable stiffness actuators. The full variable impedance actuators which allow to modify the damping too are not taken into account in our study, because they

mainly have an interest in security and humanoid robotics applications. From an energy efficient point of view, they do not bring advantages regarding the classic actuators.

Variable Impedance Actuator					
Variable Stiffness only			Variable stiffness and damping		
Modify preload of the spring	Change transmission between load and spring	Physic properties of the spring	Rheological properties	Eddy currents	Fluid dynamics

Table 2.1: Classification of the technologies for VIA [13]

This part will explain in detail the different technologies of variable stiffness actuator and highlight some that would be interesting for this master thesis.

2.3.2 Change preload of the spring

In this category, stiffness is tuned by changing the preload of the spring. there are two main subcategories, one that tries to mimic the nature using antagonistic springs. Here the motors provide both power and preolad change. The third category, preload adjustment of single spring is often composed of a principal motor providing the power and a secondary motor tuning the stiffness.

Antagonistic springs

For this type of VSA, springs and motors are placed in an antagonistic setup (figure 2.20), and non-linear springs are needed. In fact, those springs have a stiffness depending on the active length, mostly with a quadratic force-length function. These non-linear springs can be obtained by numerous methods, by having a special geometry for the spring (pitch progressive spring) or with mechanical chains using cams and pulleys.

Antagonistic springs with antagonistic motors are widely used in robotics and in humanoid robotics because they mimic the musculo-skeletal system. With this technology, actuation of the two motors in the same direction creates motion, whereas actuation in opposite direction sets different joint stiffness. The DLR QA-joint is designed according to this definition [27].

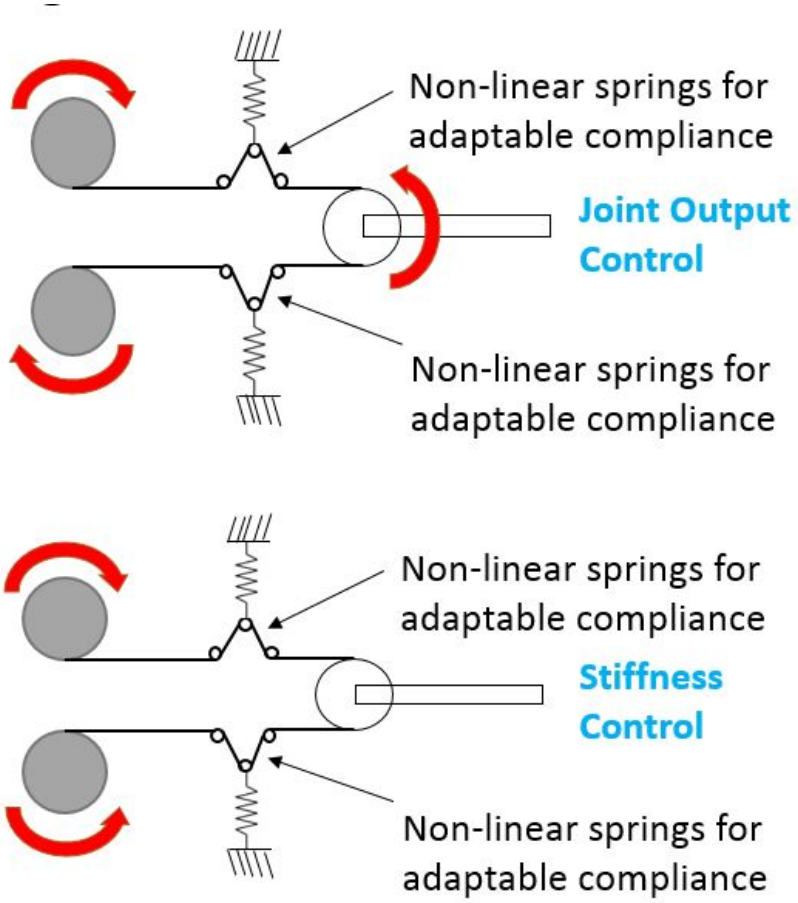

Figure 2.20: Working principle of an antagonistic setup

Preload adjustment of single spring

One of the most advanced VSA using the preload adjustment of single spring was produced by the DLR [12]. The DLR FSJ has been developed thanks to an energy based design. A big motor providing the power is linked to an harmonic gear, which is often used in VSA, because they have a high reduction ratio for a high compactness. The output of the harmonic drive is connected to a mechanical system composed of cam. The output of the joint is connected to the cam roller, and the two cam disks are linked with a floating spring. By rotating one of the cam disks (thanks to the second small motor), the authorized deviation is modified, from 3 to 15° (corresponding to a respective stiffness of 826 to 52.4 Nm/rad).

2.3.3 Change transmission between the load and the spring

In this section, the stiffness is changed thanks to the link between the output and the compliant element, without any preload. This big difference brings one advantage

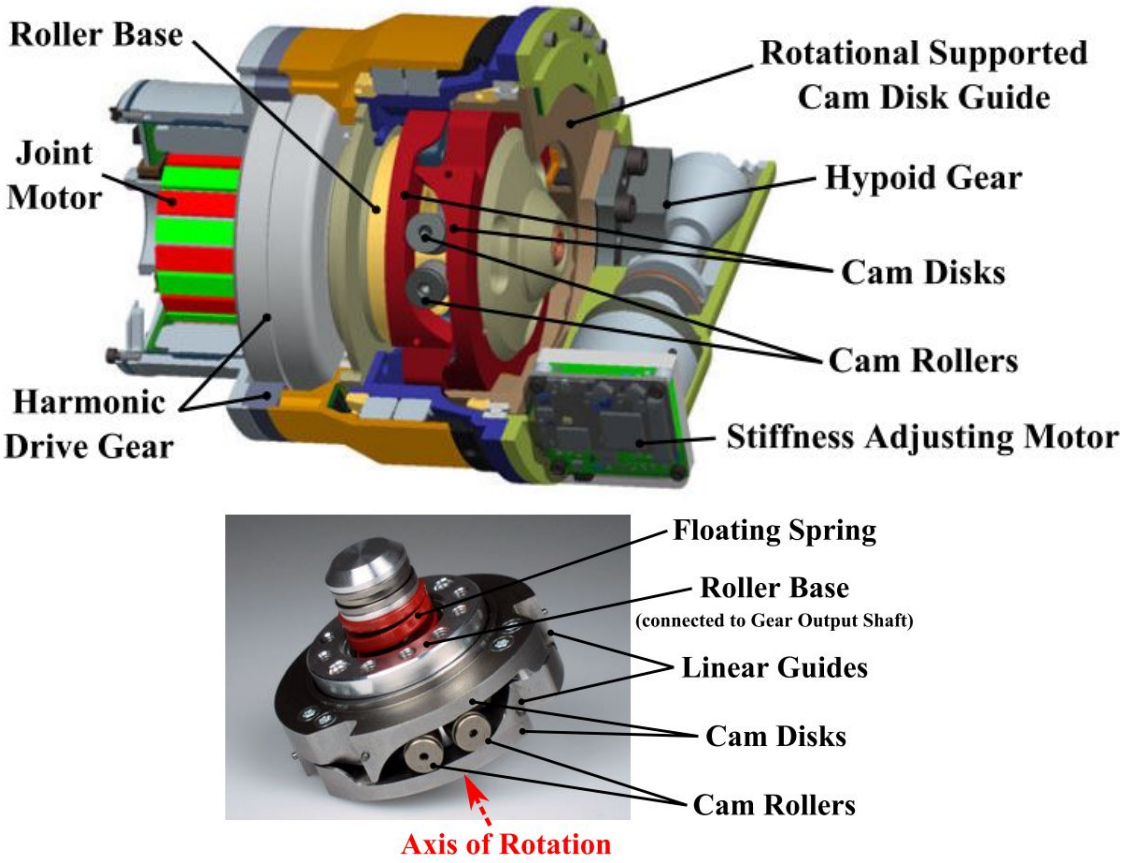

Figure 2.21: Cross section of the FSJ and physical mechanism showing the cam disks and the spring [12]

to this class of VSA : the system at equilibrium requires no power to keep a constant stiffness, which is good on an efficiency plan. Energy is still needed to tune the stiffness, with different possibilities : modify the lever length of a lever mechanism, use a non-linear mechanical link, or use continuously variable transmission between the load and the spring.

Lever length

A lever is defined by three points : A pivot, center of rotation, the point where the spring is attached and the point where the force is applying. Different compliant actuators are using lever by modifying one of these three point. Then, the relation between the force applied and the displacement is modified, and with a fixed spring, a variable stiffness actuator is obtained (figure 2.22).

This class of VSA is used in many designs as is easy to control and consumes less energy. The difficulty is in the mechanical design. The VSA-UT [14] is changing the

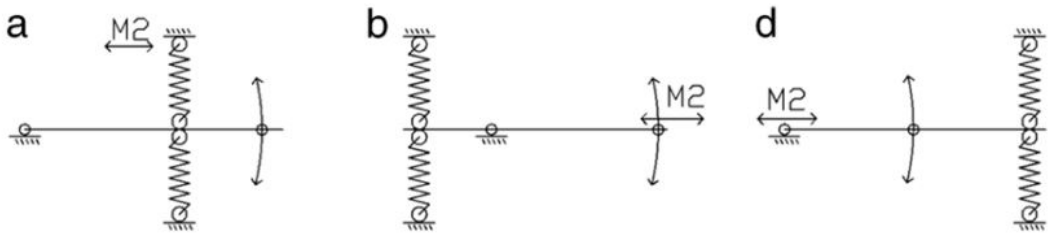

Figure 2.22: The three possibilities to modify lever length : changing spring (a), force (b) or pivot point (c) [13]

stiffness by moving the pivot point (figure 2.23) : A slide crew in M1 and M2 modify the lever length (internal DoF q_1 and q_2). The two springs are linear springs of stiffness k. Thus, the output stiffness depending on the geometric parameters is computed (by doing the partial derivative of the torque equation with respect to θ) :

$$K = 2kq_1(q_2 - l_0)\sin\theta + 2k{q_1}^2\cos 2\theta \tag{2.9}$$

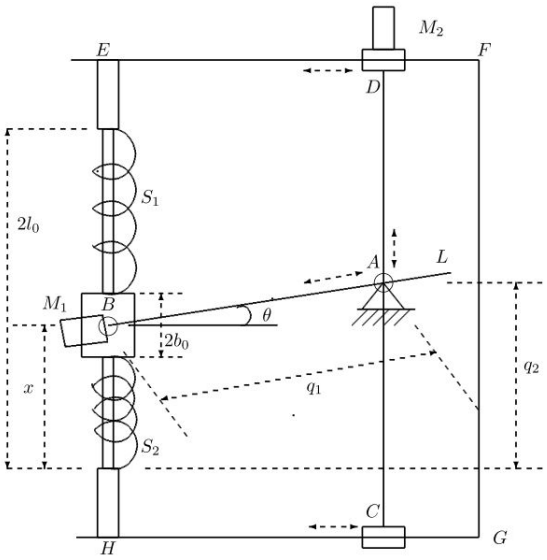

Figure 2.23: Mechanical scheme of the VSA-UT [14]

Non-linear mechanical interlink

This category of VSA is using non-linear mechanical interlink to have a stiffness dependency on the position of the mechanical interlink. Mostly the compliant elements are connected with the output thanks to pulley or cams. This category of VSA is used in some prototype of compliant hands, which often use cables and pulleys to have under-actuated motions.

Continuously variable transmission

The third approach about transmission is the use of Continuously Variable transmission (CVT), like variable diameter pulleys, toroidal or rolled based CVT. By changing the ratio between the compliant element and the load, the final stiffness of the joint is modified. There is actually no VSA based on this design even if theoretical research has been made.

However, CVTs have a utility in energy efficiency, as shown in [28]. They compared two omnidirectionnal robots, one using a classic gear reduction unit and the other a spherical continuously variable transmission. They conclude that the run-time for their robot is increased by 25% with a Spherical-CVT, which shows that it increases energy efficiency.

2.3.4 Change spring properties

The previous technologies has shown how to modify the stiffness of a VSA by acting on other components like the transmission between load and spring, the coupling between two springs, etc. The last section deals with the properties of the spring itself, and how the modification of these properties can impact the global stiffness of the actuator. In this section, not only helicoidal springs are considered, but also leaf springs, jack springs, etc.

The basic elastic law defining the stiffness is :

$$F = \frac{EA}{L_0}\Delta L \tag{2.10}$$

with F the force, E the elasticity modulus, A the cross-section area, L_0 the effective beam length and ΔL the deformation.

Elasticity modulus

Elasticity modulus is a material property which can barely be changed. The only way to change the elasticity modulus is to change the temperature of the material. As every temperature process, the inertia is important and the variation is too slow to be effective. Still some actuators named Shape Memory Alloy (SMA) are using this phenomena. The alloy is copper-aluminium-nickel or aluminium-titanium and has a quick change between its austenitic and martensitic phase. Thus, by heating the alloy, which can be made fast using Joule heating, the elasticity modulus is changed. But then the cooling takes a long time, so SMA can be used only in slow dynamics systems.

Some exploration robots using SMAs have been tested, like in [15] and [16] (figure 2.24).

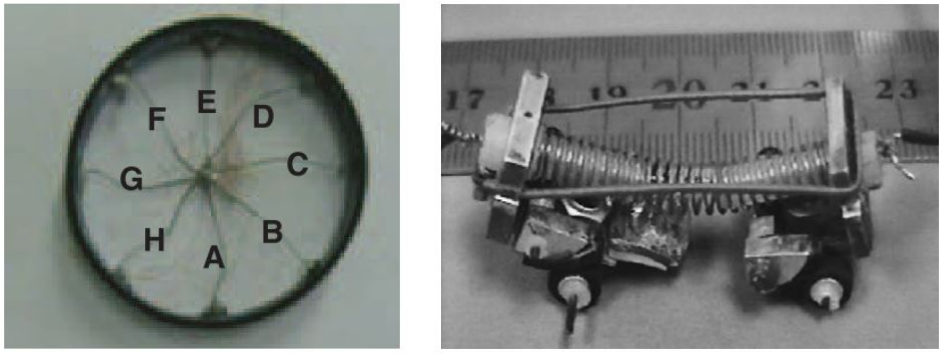

Figure 2.24: A planar rolling robot using SMA to deform its shape and crawls [15] and a wheeled robot using a sort of ≪walking bound≫ gait to move [16]

Cross section area

The idea here is to use the cross section of a beam as the parameter to change the stiffness. A non circular beam in bending is used, and by rotating the beam with a secondary motor, the cross-section area is modified. The advantage is that the power needed is small, as the effort are perpendicular to the motion. But the range of stiffness is often limited, due to the definition of the cross section area and the elastic limit. Most of the VSA designed using cross section-area propose two predefined stiffness, like a stiff and a soft position [29].

Active spring length

The last but not least way to modify the spring property is to modify the active spring length. This is the simplest way to have variable stiffness and this method has one advantage : the range of stiffness goes from a low value up to an infinite stiffness. In fact, the spring length can be modified up to zero, so the spring is totally neutralized and the VSA becomes a classic actuator, which can be interesting in some tasks. This subsection will present two compliant elements often used in VSA : the leaf spring and the jack spring.

The jack spring takes his name for the jack screw. In fact, an helical spring has the same geometry and model as a jack screw. The stiffness of a serial helical spring is the following :

$$K = \frac{Gd^4}{8D^3 n_a} \tag{2.11}$$

With G the shear modulus (a material property directly linked to the elasticity modulus), d the wire diameter and D the spring diameter. n_a is the number of active coils, the parameter modified in a jack spring.

To modify the number of active coils, a rotative element is put inside the spring. As it is helical, a rotation of this element (or of the spring) creates a translation motion and modify the number of active coils, from a minimum stiffness up to an infinite one, if the number of active coils approach zero (figure 2.25).

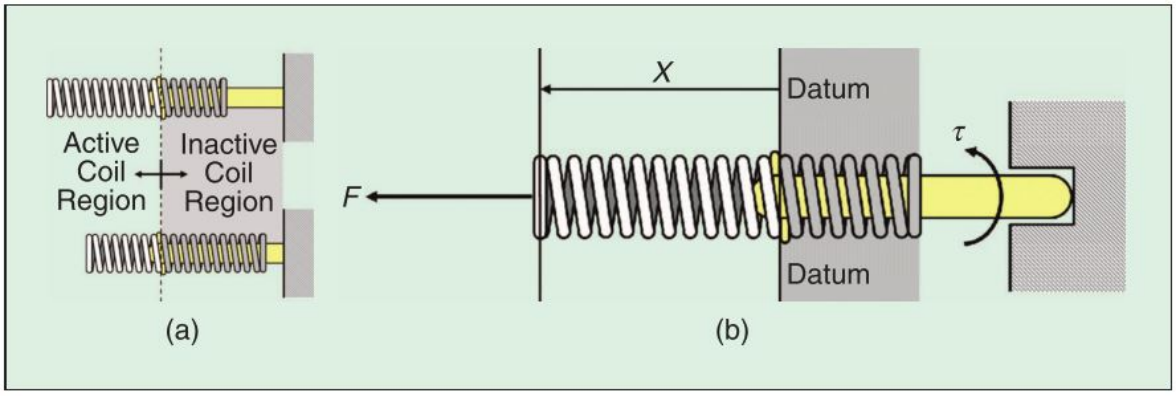

Figure 2.25: Conceptual diagram of the jack spring [17]

This actuator is quite easy to implement with an easy control, directly relying the stiffness to the length of the spring. One main drawback might be the dynamics of such a system, which can be slow regarding to antagonistic setups for instance, which can jump from a stiff state to a soft one. But depending on the tasks, this might not be a problem.

One application of the Jack spring is made in [18], where the jack spring is used as a robotic tendon (figure 2.26).

2.3.5 Conclusion

This chapter dealt with variable stiffness actuators, the different technologies and concepts to have an efficient compliant joint. This state of the art has shown that numerous way to design a VSA are possible, and almost each one has its specific application.

Antagonistic setup have the advantage to mimic the musculo-skeletal system. Thus, they are often used in humanoid robotics, thanks to their rapid dynamics and wide range of stiffness, even if they are hard to control and not very energy efficient.

Some other solutions, using the mechanical chain between load and spring, present a smart mechanic design, and several advantages : size, range of stiffness, response time, etc.

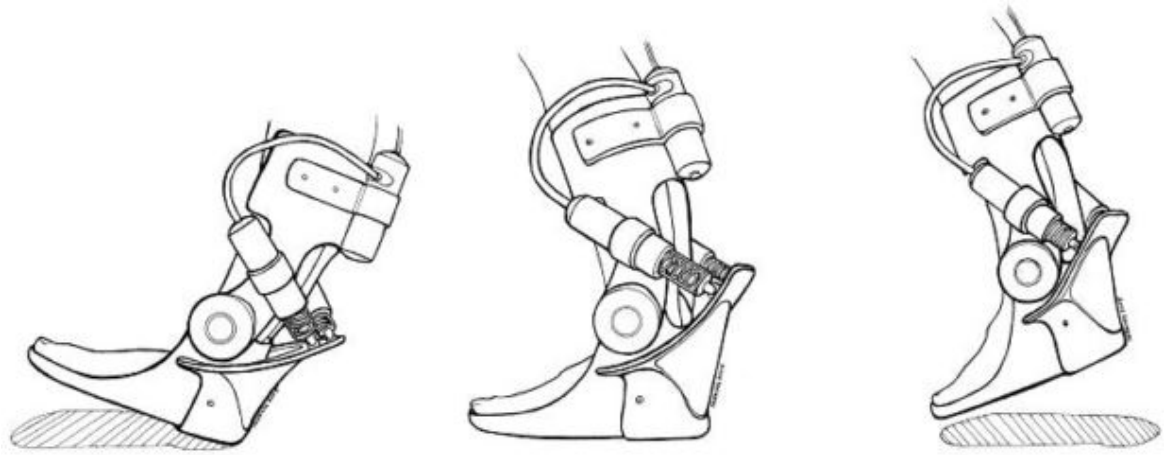

Figure 2.26: Robotic tendon using a jack spring [18]

The last section dealt with VSA acting on the physic properties of the spring. If some of them are quite hard to implement (the SMA), the other solutions seems to be the simplest one to design, such as the jack spring. This solution has one main drawback : it has slow dynamics and it is not adaptable to every system and task. For this master thesis, the aim is to find an optimal stiffness based on the resonance of the system. It needs by definition a periodic motion, on several periods to have a significant increase of energy efficiency. Thus, the tuning of the stiffness does not require to be really fast, and the jack spring could be a good design for the requirements of the exploration robot.

2.4. First conclusions regarding the bibliography work

This bibliography report presented different tools and references regarding the master thesis subject. The aim is to design an exploration robot with a high energy efficiency. The strategy chosen to obtain this high energy efficiency is to use compliant elements. By having a periodic motion of mechanical elements, mass and inertia in the system, an optimal stiffness can be found to put the system in resonance, and then reduce the energy consumption.

The first part was a state of the art about mobile robots. This subject is very large, and regarding the requirements, some categories have been put aside. One highlighted technology was the rolling robots using mobile masses, because here one can easily see the periodic aspect of the masses in the robot, and compliant elements would be quite

easy to implement in this kind of design.

The second part dealt with different strategies to reduce energy consumption. The difference has to be marked between the static and dynamic strategies. Here the interest is more in the dynamic strategies, such as the use of resonance and compliant elements to optimize the energy efficiency. Some research has already be done on the subject, showing that if the resonance principle is still the same, numerous control laws are implemented. The master thesis will focus mostly on these different control laws, to choose the optimal one for the problem.

Regarding the measure of energy consumption, the different references have shown that the energy consumed is often obtained with a simple DC motor model. The energy consumed by the secondary motor (used to modify the stiffness), slippery and other losses are almost never taken into account. This master thesis will try to find a precise way to represent more energy losses, in order to have a more accurate model of energy efficiency.

The third part was a state of the art about the variable stiffness actuators. The chronology demonstrated that the first use of compliant elements in robotic were in humanoid robots. Since, some researcher proved that using variable stiffness actuators brings more efficiency, and numerous designs have been proposed. Nevertheless, putting humanoid robots aside, few mobile robots have been designed by using compliant elements in order to increase the energy efficiency.

Regarding this report and the first conclusion made, the future work can be described as follows :

1. Modeling of robot : A rolling robot with mobile masses will be modeled. This modeling work will be made on Matlab and/or Adams. A multiphysic software like Simulink could also be used.

2. Energy efficiency analysis : Try to model the consumption of the robot previously modeled, by taking into account several parameters, the motor model included.

3. Definition of the optimal trajectory : Try to define the optimal trajectory for the robot and the actuators, based on an energy efficiency criteria.

4. Add of compliant elements : Model the robot with its variable stiffness actuators, and try to reduce the energy consumption, by computing the good variation of stiffness.

5. Definition of an adequate control strategy : Regarding all the previous work done,

an optimal control strategy will be chosen between all the control laws enunciated in this report. This control law will be test on co-simulation.

Chapter 3

Dynamic model of the robot

3.1. Introduction

This chapter will deal with the dynamic modeling of a 2D cylinder rolling on a plane. The motion is induced with three mobile masses moving along different axis. This model will be the base of work of all the thesis. The dynamic model has been computed with the Lagrangian formulation, and a corresponding model has been done on ADAMS view, in order to verify the good computation of the Lagrangian equations. The modeling of the compliant elements will be explained on the corresponding chapter.

3.2. Dynamic model of the rolling disk

3.2.1 Why choose a 2D model ?

In order to have an efficient exploration robot, the robot should have several degrees of freedom and be able to move on both directions of a plane. Some rolling spheres have been designed for this purpose [2] [3]. But the dynamics of such a robot is so complicated that Tomik et al. [30] focused on an optimal design and position of the actuators and ball-screws, that differs from the classical tetrahedral shape, in order to simplify the dynamic model and find some linearity in the model.

In fact, the interesting point of the thesis is the energy consumption and the use of compliant elements. The hypothesis that the use of VSA can perform reduction of energy consumption can be proved on a 2D cylinder. So for those reasons, we decided to first model a rolling cylinder on a plane. To be fully controllable and statically stable, the cylinder needs three actuators. We will see in the development of the dynamic model

that a 2D robot is already really complicated to model. Thus, we do not consider the 3D robot, which is a sphere with at least 4 masses, rolling on two directions. The modeling of the 3D sphere could be achieved in future work.

3.2.2 Dynamic model of the robot

The robot modeled is presented in figure 3.1, taken from [19]. It is composed of an outer shell with a cylinder shape in contact with the ground in O. The outer shell has a radius R. Three masses of mass m ($m_1 = m_2 = m_3$) are moving on their respective bar. We decided to actuate the masses with three ball-screws of reduced ratio p. The three masses are positioned with a angle difference of 120 degrees. The mass of the cylinder is neglected but we take into account its inertia J_{ds}. We also take into account the inertia J_{sc} of each screw.

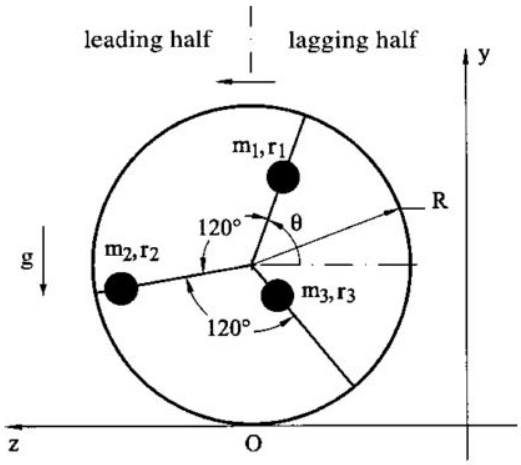

Figure 3.1: Scheme of the cylinder with three masses [19]

The first hypothesis taken is that the cylinder is perfectly rolling on the ground. Thus, the relative velocity between the center of the cylinder and the point O is zero. The motion of the cylinder can be described only with the orientation θ. The linear position of the sphere is described with r_1, r_2 and r_3, but as we have a ball-screw transmission connected to a motor, we write q_1, q_2 and q_3 the position of the motor connected to the screw, with the relation (3.1) :

$$\dot{q}_i = \frac{1}{p}\dot{r}_i \tag{3.1}$$

We want to express the dynamic model of the robot such as (3.2) :

$$\mathbf{M}(\mathbf{q})\ddot{\mathbf{q}} + \mathbf{h}(\mathbf{q}, \dot{\mathbf{q}}) = \boldsymbol{\tau}_L \tag{3.2}$$

with $\mathbf{q} = [q_1, q_2, q_3, \theta]^\top$ the vector of generalized coordinates and $\dot{\mathbf{q}}$ and $\ddot{\mathbf{q}}$ its first and second derivatives. $\mathbf{M}$ stands for the mass and inertia matrix, and $\mathbf{h}$ stands for the gravity, Coriolis and centrifugal effects. Finally, $\boldsymbol{\tau}_L = [\tau_1, \tau_2, \tau_3, 0]^\top$ is the vector of torques associated to the generalized coordinates, representing the input torque on each motor. The torque associated to θ is zero according to the perfect rolling motion, so no resistive torque is taken into account.

The dynamic model is computed with respect to the Lagrangian formulation (3.3) :

$$\frac{d}{dt}\left(\frac{\partial L}{\partial \dot{\mathbf{q}}}\right) - \frac{\partial L}{\partial \mathbf{q}} = \boldsymbol{\tau}_L \tag{3.3}$$

with L the Lagrangian, such as $L = T - V$, with T representing the kinetic energy of the system and V the potential energy of the system. So we find according (3.1), (3.2) and (3.3) :

$$\begin{pmatrix} J_q & 0 & 0 & J_{q_1,\theta} \\ 0 & J_q & 0 & J_{q_2,\theta} \\ 0 & 0 & J_q & J_{q_3,\theta} \\ J_{q_1,\theta} & J_{q_2,\theta} & J_{q_3,\theta} & J_\theta \end{pmatrix} \begin{pmatrix} \ddot{q}_1 \\ \ddot{q}_2 \\ \ddot{q}_3 \\ \ddot{\theta} \end{pmatrix} + \begin{pmatrix} h_{q_1} \\ h_{q_2} \\ h_{q_3} \\ h_\theta \end{pmatrix} = \begin{pmatrix} \tau_1 \\ \tau_2 \\ \tau_3 \\ 0 \end{pmatrix} \tag{3.4}$$

with

$$\begin{cases} J_q = J_{sc} + mp^2 \\ J_\theta = J_{ds} + 3mR^2 + mp^2(q_1^2 + q_2^2 + q_3^2) + 2mRp(q_1 \sin(\theta) + q_2 \sin(\theta + \frac{2\pi}{3}) + q_3 \sin(\theta - \frac{2\pi}{3})) \\ J_{q_1,\theta} = -mRp\cos(\theta) \\ J_{q_2,\theta} = -mRp\cos(\theta + \frac{2\pi}{3}) \\ J_{q_3,\theta} = -mRp\cos(\theta - \frac{2\pi}{3}) \end{cases}$$

and the values of the gravity, centrifugal and Coriolis contribution :

$$h_{q_i} = -mp^2 q_i \dot{\theta}^2 + mgp\cos(\theta)$$

$$\begin{aligned} h_\theta = [2mp^2(q_1\dot{q}_1 + q_2\dot{q}_2 + q_3\dot{q}_3) + 2mRp(\dot{q}_1 \sin(\theta) + \dot{q}_2 \sin(\theta + \frac{2\pi}{3}) + \dot{q}_3 \sin(\theta - \frac{2\pi}{3})) \\ + mRp\dot{\theta}(q_1\cos(\theta) + q_2\cos(\theta + \frac{2\pi}{3}) + q_3\cos(\theta - \frac{2\pi}{3}))]\dot{\theta} \\ + mgp(q_1\cos(\theta) + q_2\cos(\theta + \frac{2\pi}{3}) + q_3\cos(\theta - \frac{2\pi}{3})) \end{aligned}$$

We can see with this equation that even for a 2D rolling disk, the equations are not trivial and non-linear. That computation can explain why we have chosen to focus on

the 2D model. For the next developments, the values of the parameters are resumed in this table :

m	$1\,kg$	Weight of one mass
R	$0.3\,m$	Radius of the cylinder
J_{ds}	$0.9\,kg.m^2$	Inertia of the cylinder
J_{sc}	$8.10^{-7}\,kg.m^2$	Inertia of the screw
p	$0.0095\,m.rad^{-1}$	Reduced ratio of the ball screw

3.2.3 Matlab implementation for constant acceleration

As the system is not linear and easily solvable, a relation between the position of the mass and the position of the robot is not easy to find. In order to have a relation of this type, [19] make the assumption of a constant acceleration. They define then a periodic motion of the masses depending on θ, with some coefficients. These coefficients define the acceleration of the sphere, but as the system has several solutions, the coefficients cannot be computed for a given acceleration.

This relation has been implemented into matlab and the results are shown in figure 3.2.

For our subject, we want to show energy consumption reduction for a wide range of motion, so for non-constant acceleration trajectories. In order to find the trajectories of the mass that satisfy the dynamics of the system and the trajectory of the robot, we will use optimal principles to define adequate trajectory planner, such that minimize some cost function based on the energy cost. This part of the work will be detailed after.

3.3. ADAMS modeling of the robot : Contact modeling

In order to verify the good computation of the dynamic model, we want to model the system on ADAMS. In fact, ADAMS permits us to compare computed results to simulated one, as could do a real system. We will also use ADAMS for co-simulation and control of the robot later. If the modeling of the robot with its bodies and joints is classical, the difficult part is the modeling of the contact between the cylinder and the ground. In fact, for the computed model we decided to take the hypothesis of a no-slide rolling. In reality this is way more complex and ADAMS tries to model the

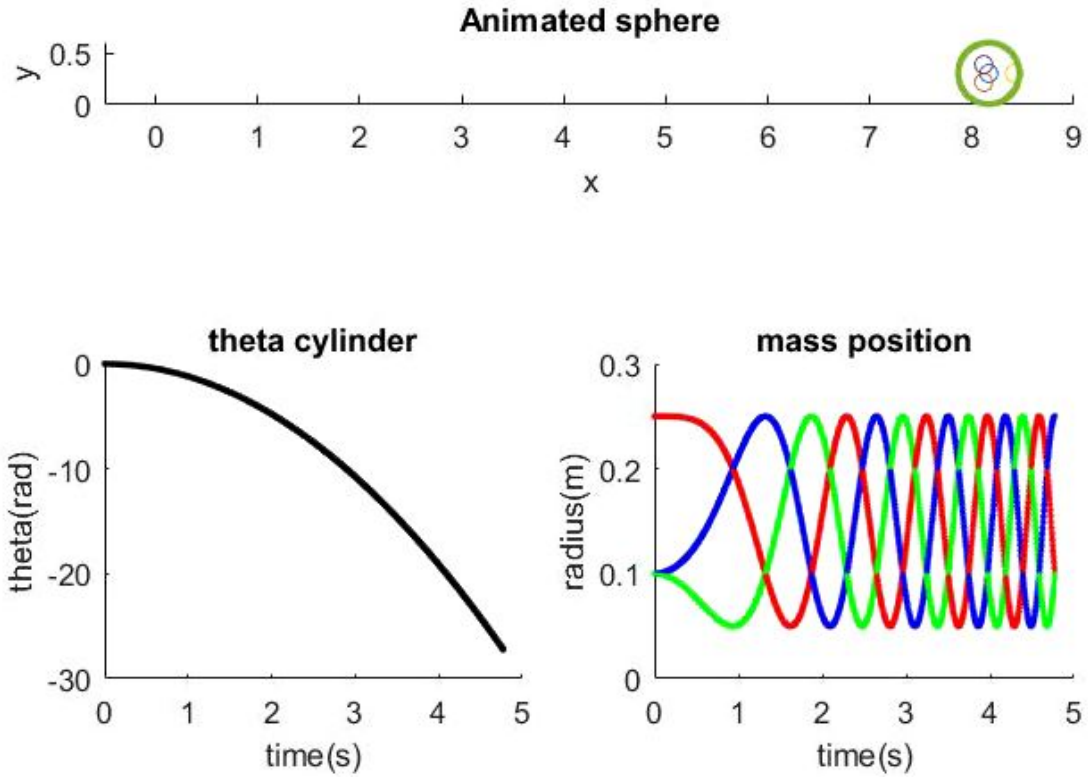

Figure 3.2: Motion of the masses for a constant acceleration

contact forces more accurately. So we need to find the good parameters in order to have a motion close to what we want to define. This modeling work is detailed in the next subsections.

The architecture of the robot has been made on solidworks, then imported as a parasolid file to ADAMS (figure 3.3). Parasolid is a 3D solid modeling component software, licensed to many independent software such as MSC software. The main advantage of parasolid is that it models geometric features with exact curvature. It means that a sphere or a cylinder for instance will have the exact shape of a sphere or cylinder and not an edged surface. Their representation is as accurate as possible and so the simulation are more close to reality. The main drawbacks lies in the duration of simulation which significantly increase with this modeling. To model using parasolid, one can design the system directly on ADAMS, or import a CAD from an other CAD software (CATIA/Solidworks) by exporting the assembly or body as parasolid files(.x_t). Then in "Settings", "solver", "contacts", "parasolid" as to be selected in order to interpret exact features for the contact and friction simulation.

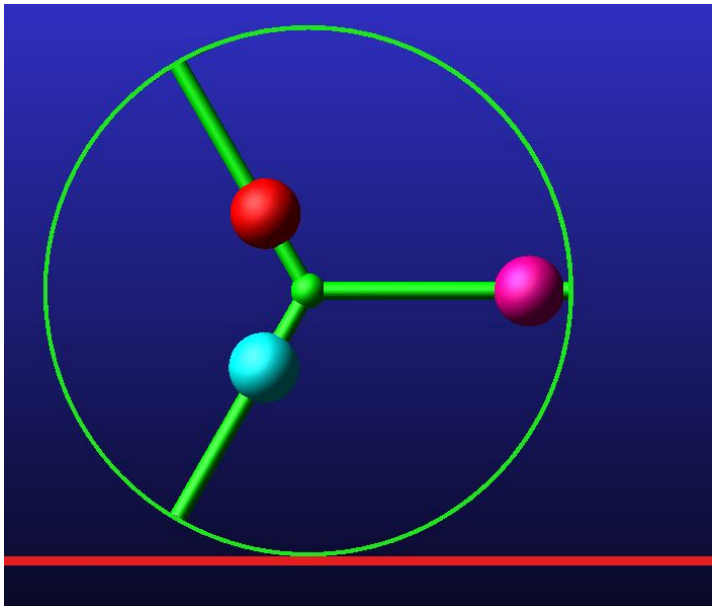

Figure 3.3: Motion of the masses for a constant acceleration

3.3.1 Theory of friction

Friction between solids is a very complicated phenomenon depending on many parameters. The most used and known model to evaluate friction is Coulomb friction. It establishes a relation between (figure 3.4a) the friction force F_f (tangential) opposed to a motion produced by the tangential force F_t of an applied force F_{app} and the normal force of contact between the two solids F_n, with a friction coefficient μ as

$$F_f = \mu F_n \tag{3.5}$$

One can differentiate static friction (stiction) and kinetic friction (sometimes called dynamic friction) with two different coefficient. As one can feel by trying to move an object on a table, the friction is more important when the object is static and then it decreases with the slipping of the object. This relation is defined by Coulomb's Friction Cone (figure 3.4b) by

$$\begin{cases} if: F_t \leq \mu_s F_n \;\rightarrow\; \mu_s \geq \dfrac{F_t}{F_n} = \tan(\theta_f) \quad \texttt{then:} \quad F_f = \mu_s F_n & (3.6) \\ \texttt{else:} \quad F_f = \mu_d F_n & (3.7) \end{cases}$$

where, μ_s is the static friction coefficient and μ_d is the kinetic friction coefficient and θ_f is the Cone angle respect the vertical. Equation (3.6) expresses the fact that if a randomly force applied onto the object (F_{app}) is not great enough, the object will remain static. While, if F_{app} is greater enough, the object will slip with an opposing force as in

(3.7). Usually, the value of the coefficient is between 0 and 1, but materials engineering is developing materials with bigger friction coefficients. Note that, as the transition between static and kinetic friction is instantaneous, in the transition a discontinuity appears.

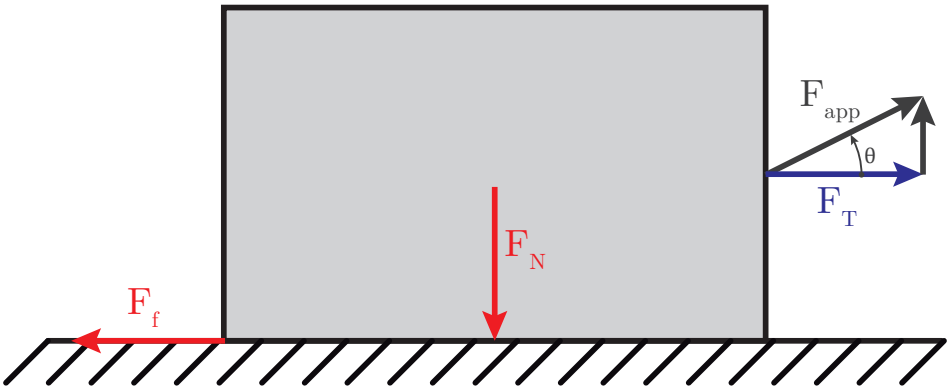

(a) Simple representation of Coulomb friction

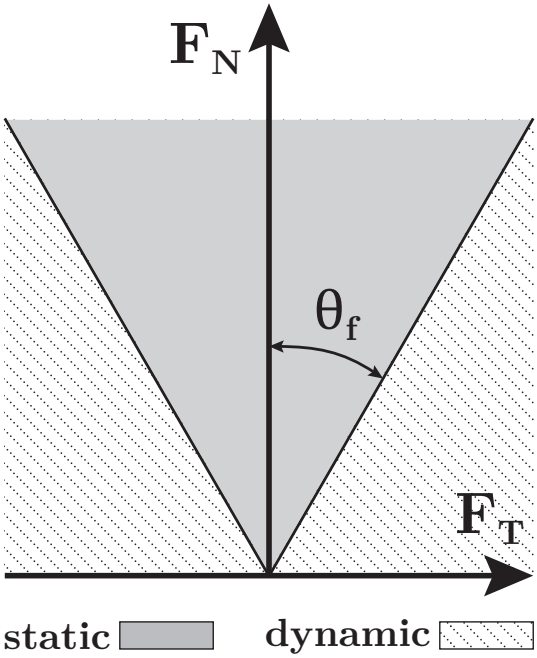

(b) Coulomb's friction cone

As it has been introduced previously, a model for the friction forces has been developed extracting it from ADAMS. The Friction force model, as presented before in equation (3.5) is :

$$F_f = \mu F_n$$

where μ is a generic value of the friction coefficient and computed in the following paragraphs.

3.3.2 ADAMS modeling of contact

In ADAMS documentation can be found the meaning of the parameters that are set by the user. As it was stated, the friction model used will be the Coulomb's model. The two first parameters refer to the already explained coefficients μ_s and μ_d. The other two parameters that one can set are the *Stiction Transition Velocity* (v_s) and the *Friction Transition Velocity* (v_d). Intuitively, by the name, one can detect that we are facing the same phenomenon as before, where the friction coefficients do not follow a continuous function (as they are different), which implies that there is a discontinuity when the object starts slipping. As introduced in the previous section, ADAMS solve this events introducing transition functions in the vicinities of the discontinuities. In the ADAMS documentation [31] is shown the chart (figure 3.5) of the friction coefficient evolution regarding the slipping velocity between the two bodies where the force is placed.

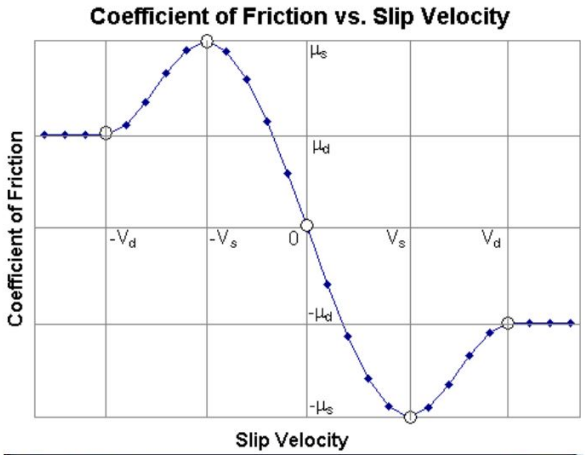

Figure 3.5: Coefficient of friction varying with slip velocity

Taking into account this graphic, in equation (3.5), the friction parameter is defined as $\mu = \mu(v_{slip})$, where v_{slip} is the slipping velocity between the two contacting objects. This antisymmetric chart can be divided in 5 sections (2 of them antisymmetric) that allow to define $\mu(v_{slip})$:

$$\begin{cases} |v_{slip}| > |v_d| & \rightarrow \mu = -sign(v_{slip})\mu_d \\ |v_s| < |v_{slip}| < |v_d| & \rightarrow \mu = -sign(v_{slip})\left[av_{slip}^3 + bv_{slip}^2 + \mu_d\right] \\ -v_s < v_{slip} < v_d & \rightarrow \mu = \left[cv_{slip}^3 + dv_{slip}^2 - \mu_s\right] \end{cases}$$

with

$$a = \frac{-2(\mu_s - \mu_d)}{(v_d - v_s)^3}, \quad b = \frac{3(\mu_s - \mu_d)}{(v_d - v_s)^2}, \quad c = \frac{-2(2\mu_s)}{(2v_s)^3}, \quad d = \frac{3(2\mu_s)}{(2v_s)^2}$$

3.3.3 Choice of the parameters

In the friction model there are some parameters that are user set. In the following paragraphs some hints are provided as how to tune them.

ADAMS provides a set of default proposed parameters. However, one must not forget that the software does not have any material context unless the properties have been given before. In order to set the friction coefficient values, experimental data can be obtained, but if this is not easy to gather, ADAMS documentation gives a table with the static and dynamic coefficients for numerous couples of materials, from where one can at least approximate the values. Two notes, the first is that, unless the materials used are special, a standard value that can be used for performing first simulations can be $\mu_s = 0.6 - 0.8$ and $\mu_d = 0.4 - 0.6$. The second remark is that, independently of the pair of values for the friction coefficients, always must be respected $\mu_s \geq \mu_d$.

Regarding the transition velocities parameters, the best way to proceed is to simulate friction behavior a first time using $\mu_s = \mu_d = 0$, in this way, the values of the slipping velocity can be read but it does not have any dynamic effect into the simulation. Once the results are obtained, one can read the values of v_{slip} when the objects are slipping and also decide when the model is considered static and read then v_{slip} again. In this way a minimum and a maximum can be obtained. Remark that this transition effect is fictitious, hence, the interest relies on obtaining a compromise between small transition zones that respect the model and stable results / quick convergence of the model. It is difficult to set generic values for these parameters because they highly depend on the model.

In the figure 3.6, we compared the actual position of the cylinder θ versus the ratio $\frac{d}{R}$ with d the horizontal displacement of the center of the cylinder. We then see that the two curves are very similar, which means that the modeling of the contact and friction is quite good.

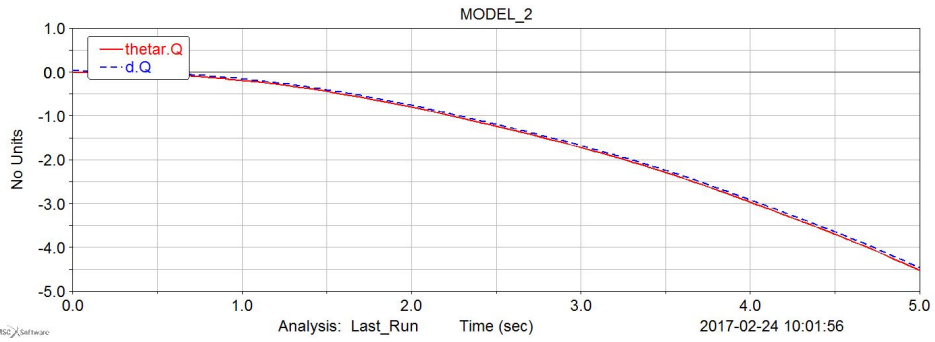

Figure 3.6: Comparison of the linear position and angular position of the cylinder

3.4. Torque computed controller for co-simulation

In order to correct the error between the computed model and the ADAMS one, we want to design a torque computed controller. The difficulty here is that the friction is between the ground and the cylinder, and that a delay appears in the motion of the cylinder, so on θ. So at one point, the computed trajectories of the masses will be dephased with the position of the sphere and the system will not roll correctly.

3.4.1 Equations for control

We want to design a PD controller according to figure 3.7. In all the subscripted names, *feed* stands for feedback and *des* for desired. The IDM block stands for the inverse dynamic model of the robot, and compute the three torques for each motor for the motion of the masses. The three torques are input of the plant and are going in the ADAMS model. The output of the plant is the angular position of the robot and its derivatives. The main difference is this controller regarding classical controller for serial or parallel robot is that the feedback variable is the position of the robot and its derivatives θ, $\dot{\theta}$ and $\ddot{\theta}$. We then remap the corresponding position of the masses and its derivatives $\mathbf{q}_{feed}$ and $\dot{\mathbf{q}}_{feed}$ in order to compute the difference between the desired and needed position of the masses. The other equations are shown in the equation (3.8). We play on the two matrices of the controller $\mathbf{K}_p$ and $\mathbf{K}_d$ in order to tune the controller properly.

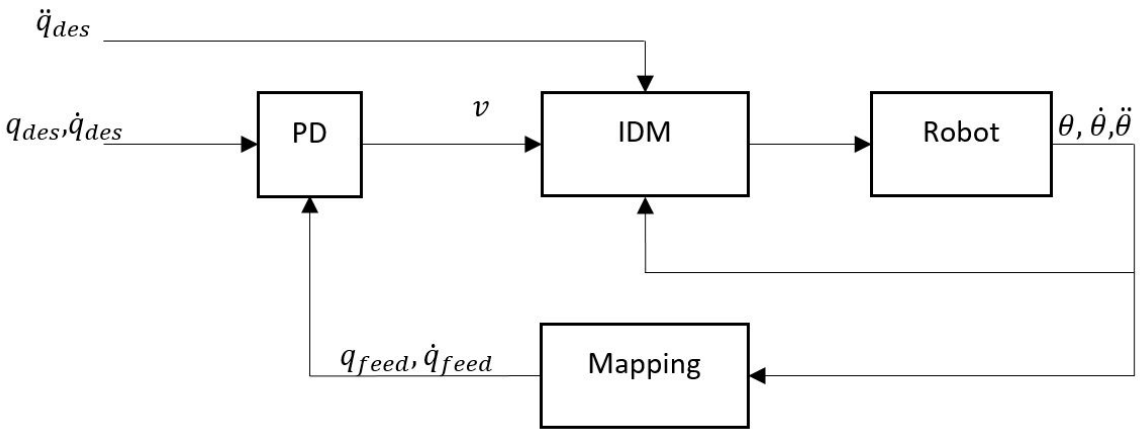

Figure 3.7: Scheme of the computed torque controller for the mobile robot

$$\begin{cases} \boldsymbol{\tau}_L = \mathbf{M}(\ddot{\mathbf{q}}_{des} - \mathbf{v}) + \mathbf{h}(\mathbf{q_{des}}, \mathbf{q_{feed}}, \dot{\mathbf{q}}_{\mathbf{des}}, \dot{\mathbf{q}}_{\mathbf{feed}}) \\ \mathbf{v} = \ddot{\mathbf{q}}_{\mathbf{feed}} = \mathbf{M}^{-1}(\boldsymbol{\tau}_L - \mathbf{h}) \\ \mathbf{v} = -\mathbf{K}_p(\mathbf{q}_{des} - \mathbf{q}_{feed}) - \mathbf{K}_d(\dot{\mathbf{q}}_{des} - \dot{\mathbf{q}}_{feed}) \end{cases} \tag{3.8}$$

3.4.2 Issues and verification

As the controller was not running at first, we directly put the desired trajectories $\mathbf{q}_{des}$ as splines for the motion of the motor, and we look on ADAMS at the induced mechanical torques. We compared those torques with the one computed by the inverse dynamic model (figure 3.8). We see that the values computed are accurate. The delay is normal because as explained before, the friction with the ground makes the system of Adams rolling slower than for the computed model where friction is not taken into account. We first thought that the controller would be able to correct those errors but it seems that they are to important in order to be compensated. But the effect of the friction might be preponderant, so the controller is not able to compensate them correctly. One solution could be to include the friction on the motor model.

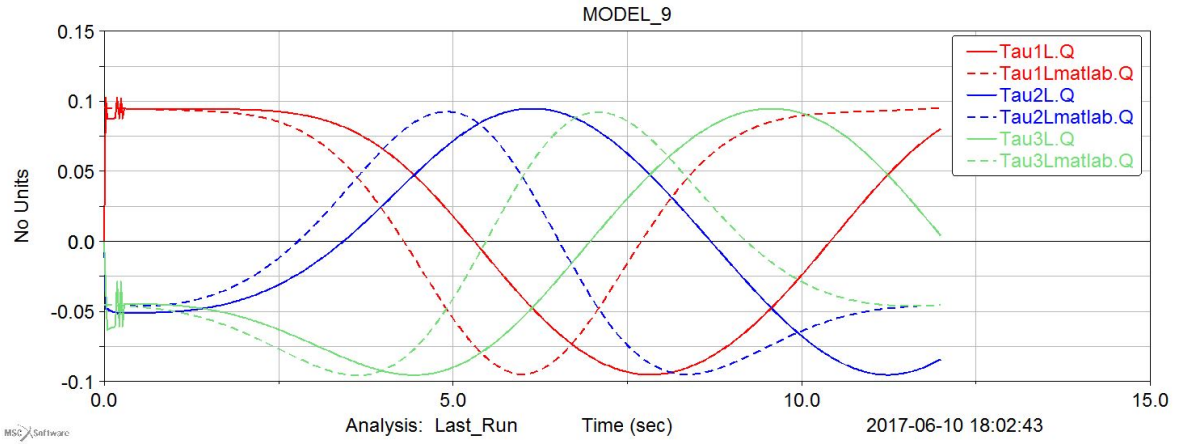

Figure 3.8: Torques induced by the motions of the mass in plain line versus the torques computed by the inverse dynamic model on matlab in dashed-line. Each color stands for one motor-mass system.

3.5. Conclusion

In this chapter, we have built the model of the 2D robot. The dynamic model of the robot is not so easy to compute, that is why we decided to built an ADAMS model

in the same time. We have verified thanks to ADAMS that our model is well defined. The main difference comes from the modeling of the contact and friction between the cylinder and the ground, which is very difficult to compute manually. Some error between the two models appears. We thought that this error could have been corrected with a PD controller, but it seems to be more complicated than this. This controller can be improved, but we wanted to move on to the main subject of the thesis, which is the energy consumption and the use of compliant elements.

Chapter 4

Optimal trajectory generation for high energy efficiency

4.1. Introduction

As seen in the previous chapter, the dynamic model of the cylinder is not easy to compute. In particular the relation between the position of the cylinder θ and the position $\mathbf{q}$ of the masses. If [19] tried to compute this relation for constant acceleration only, in our case we want to perform an kind of trajectory. One good way for this is to use optimal theory. Optimal control theory is the science of optimization [32]. The aim is to find some optimal values of variables called optimization variables in order to minimize the value of a cost function. All of this is of course done under constraints. Optimal control theory is used in various fields such as mechanical engineering, economy and robotics. In our case, the value we want to minimize in the energy consumption of the robot. So in order to have a higher energy efficiency, we will try to optimize the trajectory in order to minimize the energy losses of the robot. In order to do this, we have to compute all the possible origins of the losses. There is obvious origins like friction between bodies but a lot of losses come from the motors and associated electronics. The first section will deal with this.

4.2. Motor and consumption model

4.2.1 Electromechanical modeling of three-phase brushless motors

In order to better understand the energetic performance of robot manipulators, the modeling of the physical behavior occurring in the motors in their different operation modes has been made previously by Rafael Balderas Hill for his PhD work. The motor model used in this thesis is directly coming from his work. Based on the energetic and power performances, the motors chosen for this work were direct drive brushless-type motors. It is worth mentioning that in the absence of gear boxes in the direct drive actuators configuration, not additional mechanical losses due to friction are present.

Working principle of the three-phase brushless motor drive systems

There are two main parts to be modeled in the three-phase brushless motor drive system: the driver and the motor. The synthesized schematic of the driver and motor system is shown in figure 4.1. It can be seen that the system is divided into four parts, and each part takes care of the functioning of a specific task, as follows:

- Three-phase rectifier: Converts the three-phase AC voltage from the input line supply to a DC voltage at the output, i.e. the DC bus voltage at the node connecting the capacitor and the braking resistance;

- Braking: It is composed of a capacitor in parallel to a resistance. The capacitor store voltage to a specified limit when the current circulates in the opposite direction (braking), and the rest of the current is dissipated through the braking resistance (R_{brake}) when the switch in its line is closed;

- Voltage source inverter: It consists of a configuration of six-transistor-commutable bridge that controls the energization of each phase of the brushless motor. Moreover, a freewheeling diode is placed in parallel to each transistor in order to provide a path to release energy stored in the inductors of each phase of the motor when they are being commuted;

- Three-phase motor: The phases are placed in a Wye (Y-shaped) configuration that connects all the windings to a central point. Each phase has a resistance and an inductor in series as in any typical one-phase electric motor;

- External resistance: It can be placed optionally in the driver configuration in case higher loads must be handled by the driver system contributing to the dissipation of the energy.

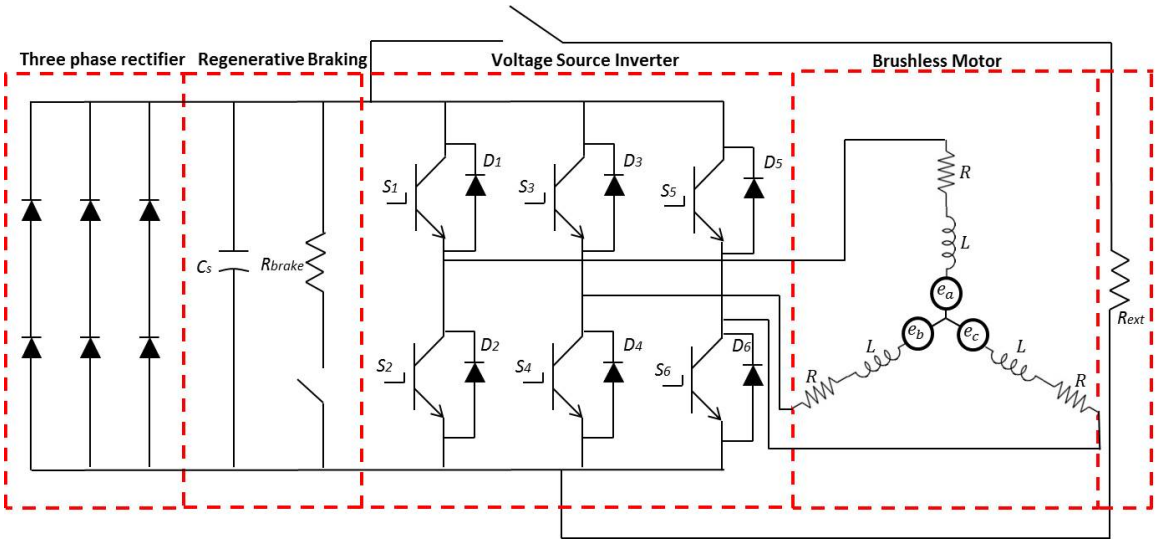

Figure 4.1: Schematic of three-phase brushless motor drive system

Modeling of the motor drive system

The modeling of the complete motor drive system is computed by splitting into the electrical part and the mechanical part.

Modeling of the electric part:

First, the state space equations of the electric part of the motor (fig. 4.2) are computed by considering the Ohm's and Kirchhoff's circuit laws [**?**] as follows:

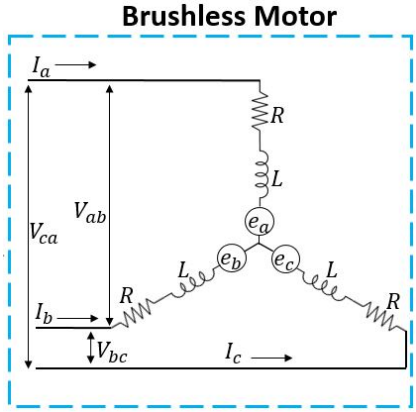

Figure 4.2: Electric circuit of the brushless motor with three phases

$$\begin{bmatrix} V_a \\ V_b \\ V_c \end{bmatrix} = \begin{bmatrix} R & 0 & 0 \\ 0 & R & 0 \\ 0 & 0 & R \end{bmatrix} \begin{bmatrix} I_a \\ I_b \\ I_c \end{bmatrix} + \begin{bmatrix} L & 0 & 0 \\ 0 & L & 0 \\ 0 & 0 & L \end{bmatrix} \frac{d}{dt} \begin{bmatrix} I_a \\ I_b \\ I_c \end{bmatrix} + \begin{bmatrix} e_a \\ e_b \\ e_c \end{bmatrix} \tag{4.1}$$

whereV_a, V_b, V_c are the phase voltages, I_a, I_b, I_c represent the stator phase currents and e_a, e_b, e_c are the back electromotive forces.

The induced back electromotive forces are displaced 120 degrees from phase to phase, and they can be modeled based on figure 4.3:

$$e_a = K_e f(\theta_e)\omega_m \tag{4.2}$$

$$e_b = K_e f(\theta_e - 2\pi/3)\omega_m \tag{4.3}$$

$$e_c = K_e f(\theta_e + 2\pi/3)\omega_m \tag{4.4}$$

With some manipulations in the equations, we obtain the electromagnetic torque pro-

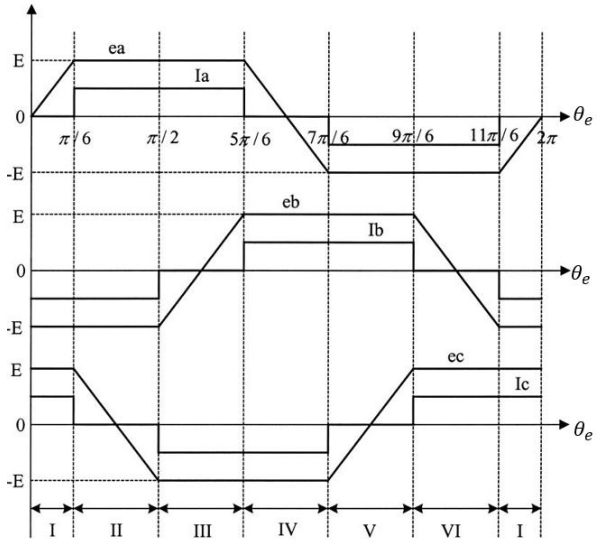

Figure 4.3: Electromotive forces

duced by the Brushless motor :

$$\tau_e = \frac{e_a I_a + e_b I_b + e_c I_c}{\omega_m} \tag{4.5}$$

Modeling of the mechanical part:

$$\tau_e = \tau_L + J\dot{\omega}_m + B\omega_m \tag{4.6}$$

where τ_L is the load torque, J is the inertia of the rotor, B is the damping factor.

4.2.2 Operation modes of the brushless motor

Based on the behavior that the load, connected to the electric motor, performs, it is possible to classify the motor performances into four different operation modes. These operation modes mainly differ one from each other depending on how the current circulates through the overall electric circuit of the motor drive system. These four operation modes are classified into motoring, freewheeling motoring mode, freewheeling generating mode and generating mode. All of them are depicted from fig. (4.4) to fig. (4.7), respectively.

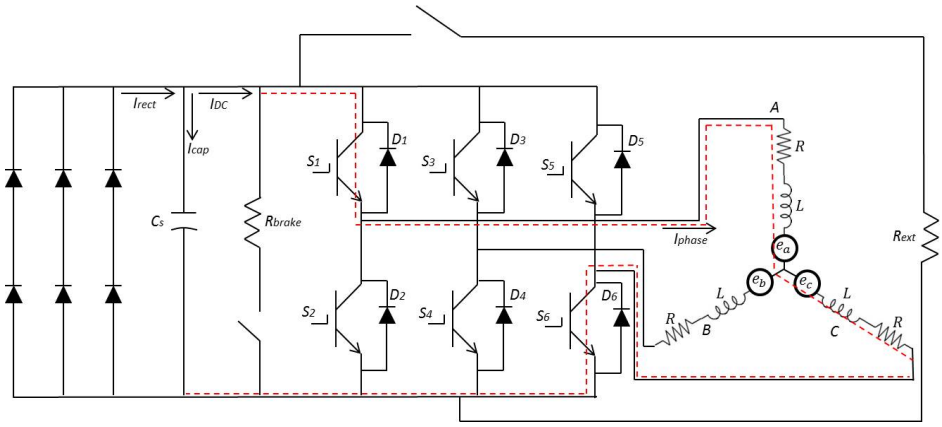

Figure 4.4: Motoring mode

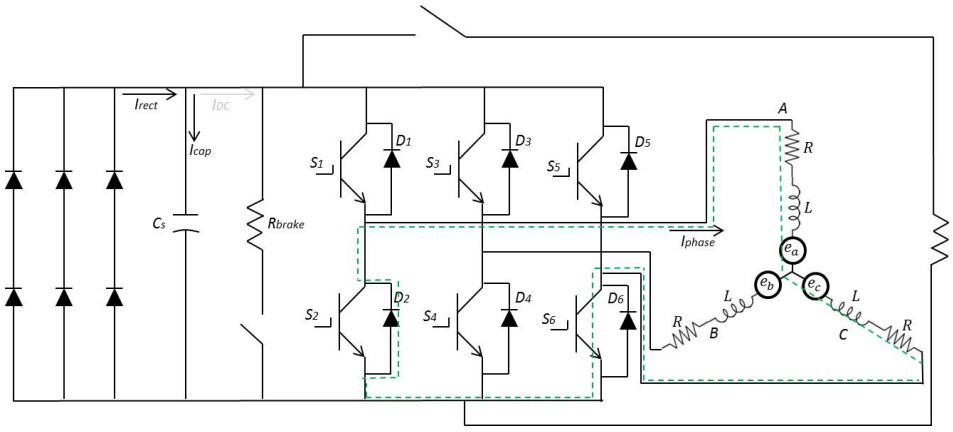

Figure 4.5: Freewheeling motoring mode

4.2.3 Modeling of the electrical and mechanical losses of the brushless motors

From the aforementioned electric-mechanical parameters and circuit configurations, different types of losses are identified:

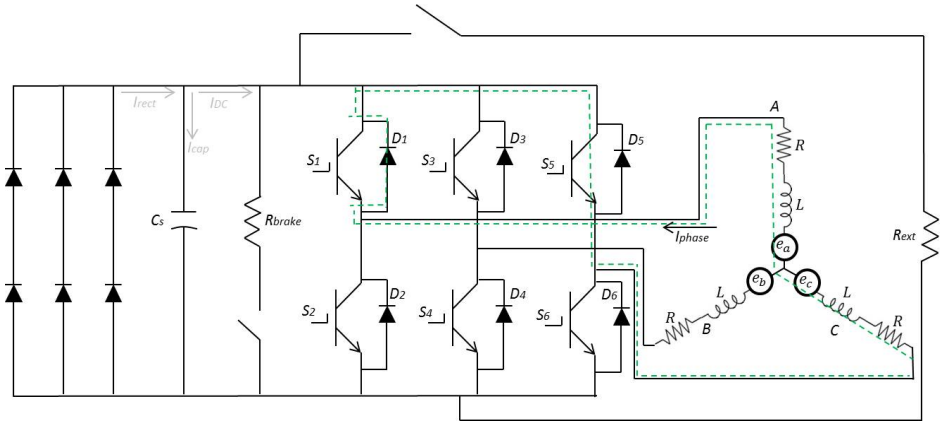

Figure 4.6: Freewheeling generating mode

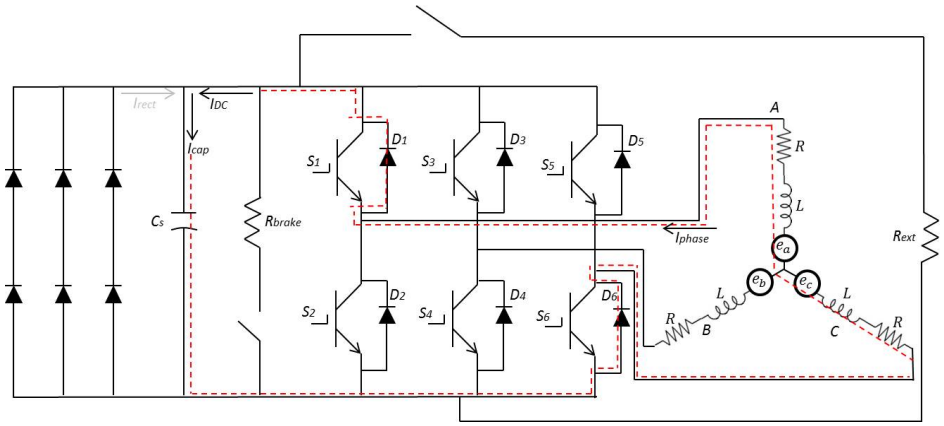

Figure 4.7: Generating mode

- Resistive losses: These are electrical losses generated in the resistance of the electric circuit of each phase of the motor, and in the braking resistance. It is worth recalling that in the generating mode of the motor, the most preponderant losses are present through the braking resistance. They can be modeled thanks to the Ohm's laws [**?**], as follows:

$$P_{res_{motor}} = RI^2 \tag{4.7}$$

$$P_{brake} = R_{brake}I^2 \tag{4.8}$$

where I is defined as the line-to-line current:

$$I = I_{LL} = I_{ph} = I_a = I_b = I_c \tag{4.9}$$

- Damping losses: These are mechanical losses that come directly from damping or friction effects and can be modeled as follows:

$$P_{damping} = B\omega_m^2 \tag{4.10}$$

- Conduction losses: The conduction losses are electrical losses due to the circulation of current through the transistors and diodes occurring in the four operation modes depending on which transistor is activated. They are modeled as follows:

$$P_{conduction} = P_{transistor_c} + P_{diode_c} \tag{4.11}$$

$$P_{transistor_c} = u_{ce} I_{c_{av}} + r_c I^2_{c_{rms}} \tag{4.12}$$

where u_{ce} is the collector to emitter voltage;
$I_{c_{av}}$ is the collector current:

$$I_{c_{av}} = \frac{V_{LL}}{V_d} I \tag{4.13}$$

r_c is the on-state resistance; $I_{c_{rms}}$ is the RMS value of the collector current:

$$I_{c_{rms}} = \frac{V_{LL}}{V_d} I^2 \tag{4.14}$$

$$P_{diode_c} = u_D I_{D_{av}} + r_D I^2_{D_{rms}} \tag{4.15}$$

where u_D Diode forward voltage;
$I_{D_{av}}$ is the diode current:

$$I_{D_{av}} = (1 - \frac{V_{LL}}{V_d}) I \tag{4.16}$$

r_D is the on-state resistance; $I_{D_{rms}}$ is the RMS value of the diode current:

$$I_{D_{rms}} = (1 - \frac{V_{LL}}{V_d}) I^2 \tag{4.17}$$

$$P_{conduction} = \underbrace{u_{ce} I_{c_{av}} + r_c I^2_{c_{rms}}}_{\text{Transistor}} + \underbrace{u_D I_{D_{av}} + r_D I^2_{D_{rms}}}_{\text{Diode}} \tag{4.18}$$

- Switching losses: Due to the continuous switching in the six-transistor-commutable bridge, electrical losses are generated in the transistors and the freewheeling diodes.

$$P_{switching} = P_{transistor_s} + P_{diode_s} \tag{4.19}$$

$$P_{transistor_s} = u_{ce} I_c f_{sw} \tag{4.20}$$

$$P_{diode_s} = u_D I_D f_{sw} \tag{4.21}$$

f_{sw} is the switching frequency

- Rectification losses: These losses come from the supply part of the driver system, specifically from the diodes in the bridge rectifier (Three-phase rectifier). They are modeled same as expression 4.15.

$$P_{rectifier} = u_{DR} I_{DR_{av}} + r_{DR} I^2_{DR_{rms}}$$

4.2.4 Motor model on simulink

A multi physics model of the brushless motor has been done on simulink. It includes a modeling of a speed controller and current controller, and the modeling of all the electronics like the source of energy for electrical network, the three phase inverter, the brushless motor. Those blocks use components from electronic libraries that needs very little time step such as $10^{-6}\,s$. So the simulation is very heavy and only short simulations can be performed.

The input of the system is both the desired speed and mechanical input torque from the system. The model then compute all the potentials and currents for each phase of the motor, the electronic torque and other parameters used to determine the operating mode of the motor.

All this variables are then used to compute the power consumption of the motor and its electronics.

4.2.5 Power consumption modeling

Thus, after all losses have been modeled, it is possible to group the overall loss balance into the following model:

$$P_{losses} = P_{rectifier} + P_{switching} + P_{conduction} + P_{res_{motor}} + P_{Brake} + P_{damping} \tag{4.22}$$

$$P_{losses} = \underbrace{u_{DR} I_{DR_{av}} + r_{DR} I^2_{DR_{rms}}}_{\text{Supply}} + \underbrace{u_{ce} I_c f_{sw} + u_D I_D f_{sw} + u_{ce} I_{c_{av}} + r_c I^2_{c_{rms}} + u_D I_{D_{av}} + r_D I^2_{D_{rms}}}_{\text{Transistor and diode}} + \underbrace{RI^2 + B\omega_m^2}_{\text{Motor}} + \underbrace{R_{Brake} I^2}_{\text{Braking}}$$

Finally, the total power consumption model can be expressed by the following equations:

$$P_{total} = P_{mech} + P_{losses} \tag{4.23}$$

$$P_{total} = \underbrace{P_{mech}}_{\text{Output}} + \underbrace{P_{rectifier}}_{\text{Supply}} + \underbrace{P_{switching} + P_{conduction}}_{\text{Transistor and diode}} + \underbrace{P_{resistive} + P_{damping}}_{\text{Motor and braking}} \tag{4.24}$$

$$P_{total} = \underbrace{\tau_e \omega_m}_{\text{Output}} + \underbrace{u_{DR} I_{DR_{av}} + r_{DR} I^2_{DR_{rms}}}_{\text{Supply}} + \underbrace{u_{ce} I_c f_{sw} + u_D I_D f_{sw} + u_{ce} I_{c_{av}} + r_c I^2_{c_{rms}} + u_D I_{D_{av}} + r_D I^2_{D_{rms}}}_{\text{Transistor and diode}} + \underbrace{RI^2 + B\omega_m^2}_{\text{Motor}} + \underbrace{R_{Brake} I^2}_{\text{Braking}} \tag{4.25}$$

4.2.6 Identification of the motor

As said before, the simulink model of the motor includes electronics parts from special libraries that needs very little time-step to work correctly. As we need for our optimal problem a very fast computation of the losses, we will simplify the motor model. The simulink model, which is very accurate and allows us to see the origin of each loss, will be used further in order to verify our results. Lee and al. define all the losses as follow [8] :

$$P_{losses} = \sum_{i=1}^{n} (\kappa_i^a |\tau_i| + \kappa_i^b \tau_i^2) \tag{4.26}$$

with n the number of actuators, κ^a and κ^b coefficients relative to the motor. Here, the three actuators are the same so just the value of the torque is changing from one to another.

We obtained the coefficients κ^a and κ^b by identification with the motor model. For a fixed desired speed, we put different desired constant torques, and then use a tendency equation in order to find the parameters (figure 4.8):

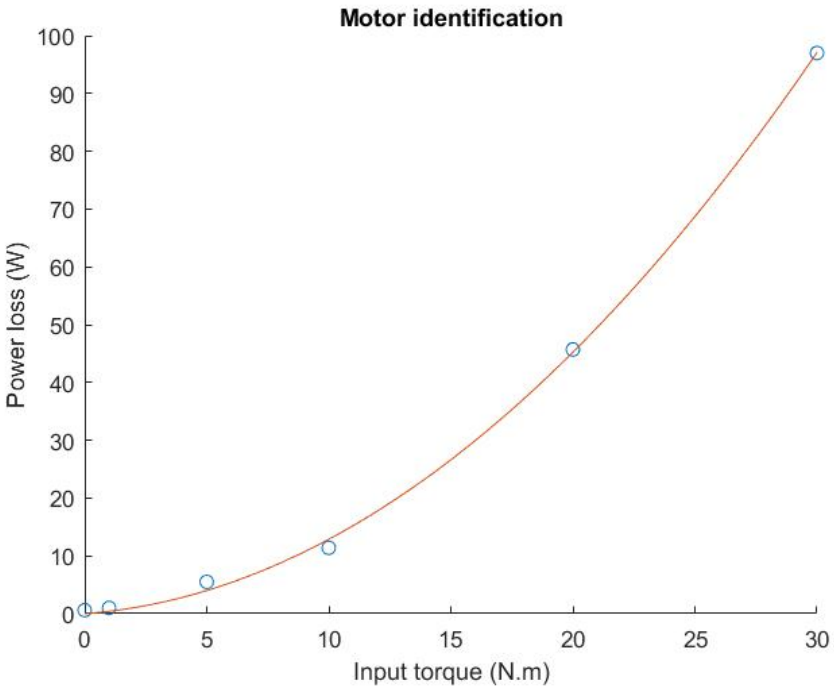

Figure 4.8: Identification of the motor parameters

We then found the following values :

$$\begin{cases} \kappa^a = 0.5822 \\ \kappa^b = 0.0912 \end{cases} \tag{4.27}$$

This value will be used in the objective function of the optimal problem.

4.3. Optimal problem

4.3.1 Definition of the optimal problem

For a given trajectory of the robot $(\theta, \dot{\theta}, \ddot{\theta})$, we want to find the trajectories of the masses, that minimize the energy consumption of the robot. Of course those trajectories have to respect some constraints such as the respect of the dynamic model, some bounds for the trajectories and maximal torques.

In our case, we can define the cost function as the following (4.28):

$$E(\mathbf{q}(\boldsymbol{\alpha})) = \int_0^T P_{losses} dt \tag{4.28}$$

with $\mathbf{q}$ the angular position of each motor linked to a single mass, $\boldsymbol{\alpha}$ the vector of optimization variables, P_{losses} the losses of the system expressed in (4.8) and T the final time of the trajectory, which is fixed.

The input trajectory is the trajectory of the cylinder, and the constraints are (4.29) :

$$\begin{cases} \mathbf{M}(\mathbf{q})\ddot{\mathbf{q}} + \mathbf{h}(\mathbf{q}, \dot{\mathbf{q}}) = \boldsymbol{\tau}_L \\ \mathbf{q}p \in [0, R]^3 \\ \mid \boldsymbol{\tau}_e \mid \leq \boldsymbol{\tau}_{emax} \end{cases} \tag{4.29}$$

The dynamic model has to be respected at any time, the masses have to move between the center and the extremity of the cylinder, and the electromagnetic torque can't be higher than a given value.

So a full script on matlab has been written. It includes all the parameters for the robot and the motor, the definition of the robot trajectory. Then we used the function *fmincon* which takes several arguments, such as the objective function which is here the computation of the energy losses, the state vector for optimization. All the parts concerning the constraints and the bounds were put in the non-linear constraint function. Some options permit us to choose the minimum-search algorithm, but the default algorithm *"interior-point"* gave the best results. The last part of the script

draw all the results for the optimal solution found. It also converts the trajectories in *timeseries* file that can be used in simulink.

4.3.2 Results for bang-bang trajectory

We first wanted to test the optimization problem for constant acceleration and bang-bang trajectories. We define the robot trajectory as follows :

$$\begin{cases} \theta(t) = \frac{1}{2}at^2 \\ \dot{\theta}(t) = at \\ \ddot{\theta}(t) = a \end{cases} \tag{4.30}$$

As mentioned before, the trajectory of the mass is not known. We assume that it will be periodic and depends on the position of the robot θ, and that the trajectory will oscillate between 0 and R. We choose the following pattern for the mass trajectories :

$$\begin{pmatrix} q_1 \\ q_2 \\ q_3 \end{pmatrix} = \begin{pmatrix} \alpha_1 \\ \alpha_2 \\ \alpha_3 \end{pmatrix} + \begin{pmatrix} \alpha_4 & 0 & 0 \\ 0 & \alpha_5 & 0 \\ 0 & 0 & \alpha_6 \end{pmatrix} \begin{pmatrix} \cos(\theta) \\ \cos(\theta + 120°) \\ \cos(\theta - 120°) \end{pmatrix}$$

with α_i the optimization variables.

The trajectory of the masses is shown in figure 4.9a and 4.9b. We see that the amplitude of the motion is depending on the value of the acceleration. For little acceleration the masses are not moving a lot whereas they are using the all possible range of motion for higher acceleration. We also saw that due to this and depending on the robot parameters (weight of the mass, inertia parameters,...), a maximal acceleration of the cylinder is attainable Above this value, the mass should go above the maximum distance reachable R, which is not possible. In this case, the algorithm does not converge so we have to make sure that we don't go over this limit. This observation will be useful for more complex trajectories.

This first test of the optimization script has shown that it was converging well and that the result was accurate, with respect to the dynamic model.

4.3.3 Results for more complex trajectory

In order to avoid discontinuities in the robot trajectory, we want to have a more smooth trajectory. A classic way to do is to have a fifth-order polynomial for the position (4.31). The definition of the trajectory is given by the limit conditions. The two only conditions

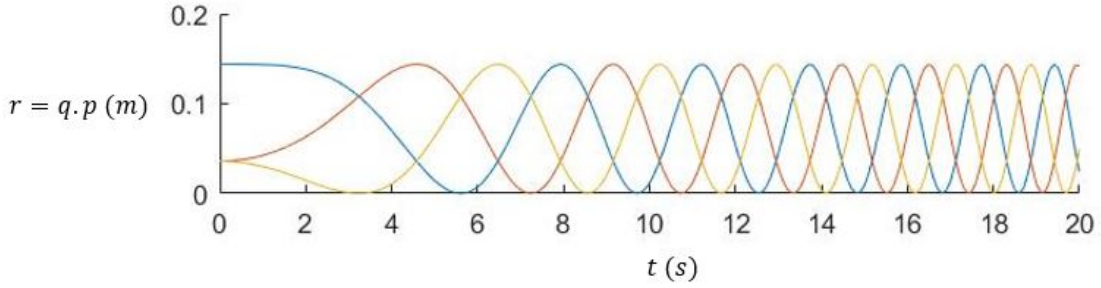

(a) Motion of the masses for an acceleration of the robot of $0.2\,m.s^{-1}$

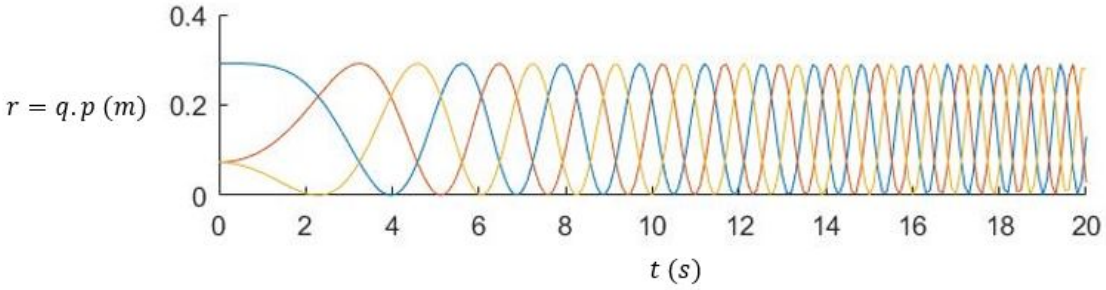

(b) Motion of the masses for an acceleration of the robot of $0.4\,m.s^{-1}$

that makes the trajectory change is the final time and final position of the cylinder. The value of each parameter of the polynomial has been calculated with formal calculation.

$$\begin{cases} \theta(t) = a_5t^5 + a_4t^4 + a_3t^3 + a_2t^2 + a_1t + a_0 \\ \dot{\theta}(t) = 5a_5t^4 + 4a_4t^3 + 3a_3t^2 + 2a_2t + a_1 \\ \ddot{\theta}(t) = 20a_5t^3 + 12a_4t2 + 6a_3t + 2a_2 \end{cases} \tag{4.31}$$

The reference trajectory chosen for the following studies is a two round trajectory over 8 seconds (figure 4.10). This is a short time in order to make the algorithm converge quickly, and also to be able to use the trajectories generated in the motor model, which supports only short simulations. With a two rounds trajectory, the maximal acceleration reached was not too important.

As seen before for a constant acceleration trajectory, we saw that the value of acceleration had an impact of the range for the motion of the cylinder. So we decided to add a dependency of $\ddot{\theta}$ for the mass trajectory pattern :

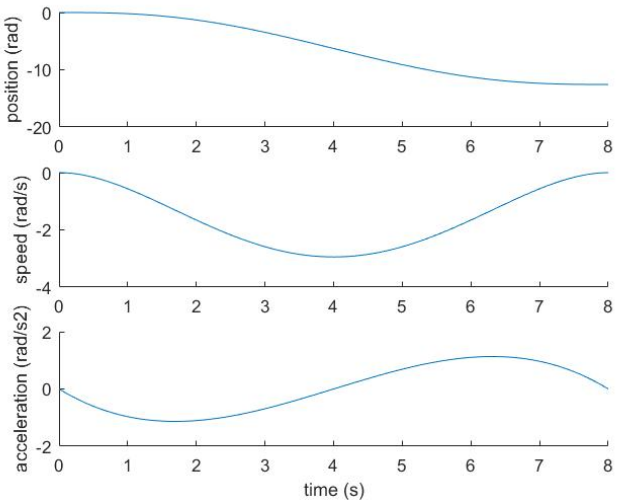

Figure 4.10: Trajectory of the robot

$$\begin{cases} q_1(\theta) = (\alpha_1\ddot{\theta}^3 + \alpha_2\ddot{\theta}^2 + \alpha_3\ddot{\theta} + \alpha_4) + (\alpha_5\ddot{\theta}^3 + \alpha_6\ddot{\theta}^2 + \alpha_7\ddot{\theta} + \alpha_8)\cos(\theta) \\ q_2(\theta) = (\alpha_9\ddot{\theta}^3 + \alpha_{10}\ddot{\theta}^2 + \alpha_{11}\ddot{\theta} + \alpha_{12}) + (\alpha_{13}\ddot{\theta}^3 + \alpha_{14}\ddot{\theta}^2 + \alpha_{15}\ddot{\theta} + \alpha_{16})\cos(\theta + 120°) \\ q_3(\theta) = (\alpha_{17}\ddot{\theta}^3 + \alpha_{18}\ddot{\theta}^2 + \alpha_{19}\ddot{\theta} + \alpha_{20}) + (\alpha_{21}\ddot{\theta}^3 + \alpha_{22}\ddot{\theta}^2 + \alpha_{23}\ddot{\theta} + \alpha_{24})\cos(\theta - 120°) \end{cases} \tag{4.32}$$

After the computation of the optimal problem, we get the trajectories of the masses (figure 4.11). We see that the range of motion is changing with the acceleration.

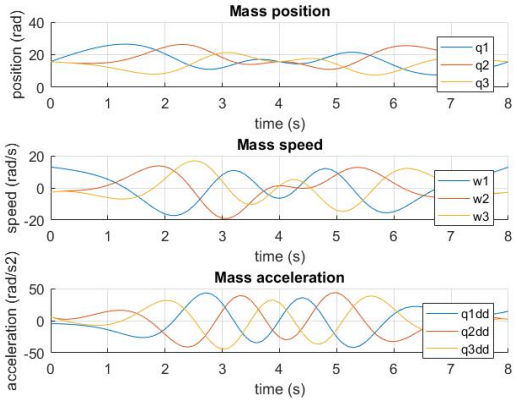

Figure 4.11: Trajectory of the masses

We also compute the mechanical input torque $\boldsymbol{\tau}_L$ and the electromagnetic torque $\boldsymbol{\tau}_e$ (figure 4.12). We can see here that the input torque remains quite constant during the simulation, because the main origin of the torque is the gravity. The electromagnetic torque is higher due to acceleration of the masses and friction in the joint (4.6).

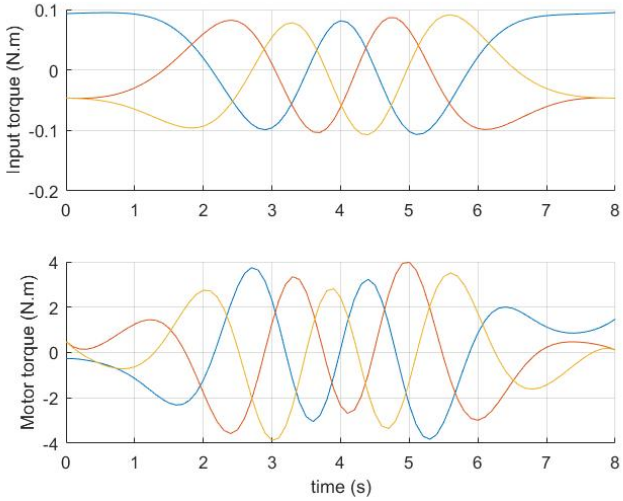

Figure 4.12: Input and electromagnetic torque

This section permitted us to rely the trajectory of the mass to the trajectory of the cylinder without solving tedious and non-linear equations. The trajectory generated is also the one minimizing the energy cost.

4.4. Energy losses

Once we have computed the optimal trajectory of the masses and the mechanical torques, we can input this datas in the motor model. We then run the simulation and plot the energetic losses along the robot trajectory (figure 4.13). We see on this graph that the energy losses are increasing non linearly. The big increase appears when the motor has to dissipate energy due to braking of the mass especially. This is this amount of energy that we want to store thanks to compliant elements and this is where we can improve the energy consumption of the system.

4.5. Conclusion

This chapter dealt with all the modeling of losses. We used a motor model defined by Rafael Balderas Hill, which takes into account the electronical and mechanical losses. We then defined an optimization problem, to find the best trajectory of the masses minimizing the energetic cost function. To have a faster algorithm, we simplified the computation of the energy losses by making a motor identification. All the results obtained have been verified on the fully accurate motor model on simulink. The next

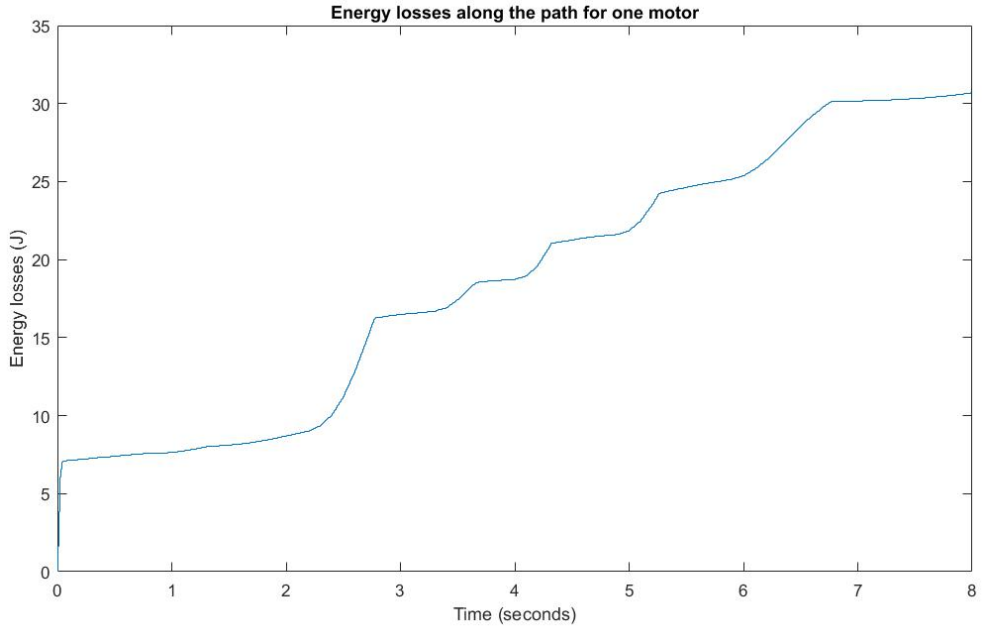

Figure 4.13: Energetic losses for one motor

step is to compare the consumption of this "nominal" robot with a "compliant" robot, using first fixed stiffness springs and then variable stiffness actuators.

Chapter 5

Add of compliant elements, impact on the energy efficiency

5.1. Introduction

As seen in the bibliography, the use of compliant elements is studied for some decades now, because it can theoretically solve several problems in robotics. In bio-inspired robotics, it can permits systems to mimic better the limbs behavior with stiff and soft properties. One other advantage is that the compliant elements can potentially store energy without losses and release it.

For this thesis we will follow the same path that the researchers followed on compliant elements. We will first model constant stiffness and try to show that for a given trajectory, an optimal stiffness exists, which permits to already reduce energy. We will then focus on the use of a compliant actuator without focusing on technology aspects. A variable stiffness system will be modeled and we will try to evaluate the energy consumption reduction, by taking into account all the losses, in the main motor and in the auxiliary motor for the variable compliance.

5.2. Modification of the dynamic model

Here, we did not take any technological and implementation aspect for the compliant elements. The aim is to prove the concept of higher energy efficiency with the use of VS. So we assume that perfect springs are used. We will see after how the stiffness is modified. As we use ball-screws systems, both linear and torsional springs can be used (figure 5.1a and 5.1b), because a ball-screw system is invertible. The changes in the

dynamic model are not so important because only the ratio of the ball-screw changes the expression of the spring related to the torque. We took torsional spring for the study. We can also choose to put springs in series or in parallel (figure 5.2a and 5.2b). In series, one need to compute as much more equation in the dynamic model for each spring, whereas in parallel the springs effect is added in the existing equations, so for simplification reasons we chose to use springs in parallel with the motor and the load.

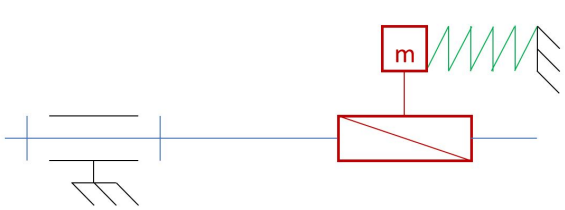

(a) Ball-screw system with a linear spring in parallel

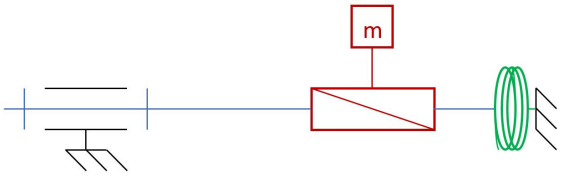

(b) Ball-screw system with a torsional spring in parallel

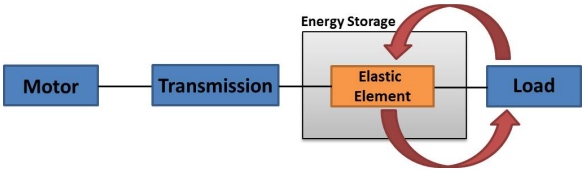

(a) Compliant element in series with the motor and the load

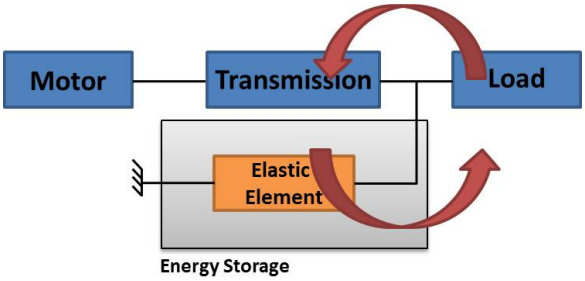

(b) Compliant element in parallel with the motor and the load

The main two aspects of VSA are physical aspect and control aspect. For control aspect, several type of controls exists and some need non-linear relation between force and displacement. Here, we mainly focus on the dynamics of the system so on physical aspects, that is why we use a fixed stiffness and position control with linear force/displacement relation, which means that we don't need a non-linear relation between the force and displacement.

In this condition, the dynamic model is the following :

$$\boldsymbol{\tau}_L = \mathbf{M}(\mathbf{q})\ddot{\mathbf{q}} + \mathbf{h}(\mathbf{q}, \dot{\mathbf{q}}) + \mathbf{K}(\mathbf{q} - \mathbf{q}_s)$$

$$\mathbf{K} = \begin{pmatrix} K_1 & 0 & 0 & 0 \\ 0 & K_2 & 0 & 0 \\ 0 & 0 & K_3 & 0 \\ 0 & 0 & 0 & 0 \end{pmatrix}$$

with $\mathbf{q}_s$ the position of the variable stiffness actuator. For a fixed stiffness compliant element, this value is the position of the spring without load. $\mathbf{K}$ is the stiffness matrix. For obvious reasons of balancing of the dynamic system, the fixed stiffness on each motor is the same, only the position of the variable stiffness actuator is different from one to another and will be computed using optimal theory as we did for the masses trajectories.

We also compute the mechanical torque applied on the auxiliary motor :

$$\boldsymbol{\tau}_s = \mathbf{J}_{vsa}\ddot{\mathbf{q}} - \mathbf{K}(\mathbf{q} - \mathbf{q}_s)$$

with $\mathbf{J}_{vsa}$ the inertia of the mechanical part of the VSA. This torque will be useful to compute the energy losses of the VSA part.

5.3. Improvement of energy efficiency for constant stiffness

5.3.1 Optimal problem

The first study on compliant elements was focused on fixed stiffness springs. We wanted to show that for a given trajectory, it exists an optimal stiffness on an energy aspect, which means that this is the stiffness for which the energy losses are minimal. This optimal stiffness principle is already used in some exoskeleton for instance where compliant elements are chosen for a given person walking at a given speed. Out of this working mode, the stiffness is not optimal anymore. The need of variable stiffness elements appears here, because we want our robot to have an high energy efficiency for all its trajectories. We recall the dynamic model of the robot :

$$\boldsymbol{\tau}_L = \mathbf{M}(\mathbf{q})\ddot{\mathbf{q}} + \mathbf{h}(\mathbf{q}, \dot{\mathbf{q}}) + \mathbf{K}(\mathbf{q} - \frac{R}{2p})$$

but here, as there is not variable stiffness device, the position of the spring without load is fixed and chosen to be in the middle of the possible motion range.

The new optimal script is the following :

1. We first run a script for all the given values : Parameters of the model, of the robot, and desired trajectory of the robot.

2. We then run the optimization script which is the same as before, computing the optimal trajectory of the masses, based on a energetic criteria presented before.

3. We then run an other optimization function but this time, the mass trajectory computed before is given, the only optimization variable is the stiffness. The function optimize this stiffness for the mass trajectory given, still based on the minimal energy losses criteria.

4. The last part of the script stores all the data and plot results.

For the given robot trajectory mentioned before, we find an optimal stiffness of $k = 0.2589\, N.m.rad^{-1}$ which is an acceptable value for this type of spring.

We can compare with those results the mechanical torques for the normal system and the system with the optimal stiffness (figure 5.3). We see that the mechanical torques are way higher than for the classic system. This could appear counter intuitive for an energy consumption point, but in fact the peaks of torques appear in the good moment, because it's when the mass needs to accelerate. So this increase in the mechanical torque works as a decrease in the electromagnetic torque on the actuator (figure 5.4).

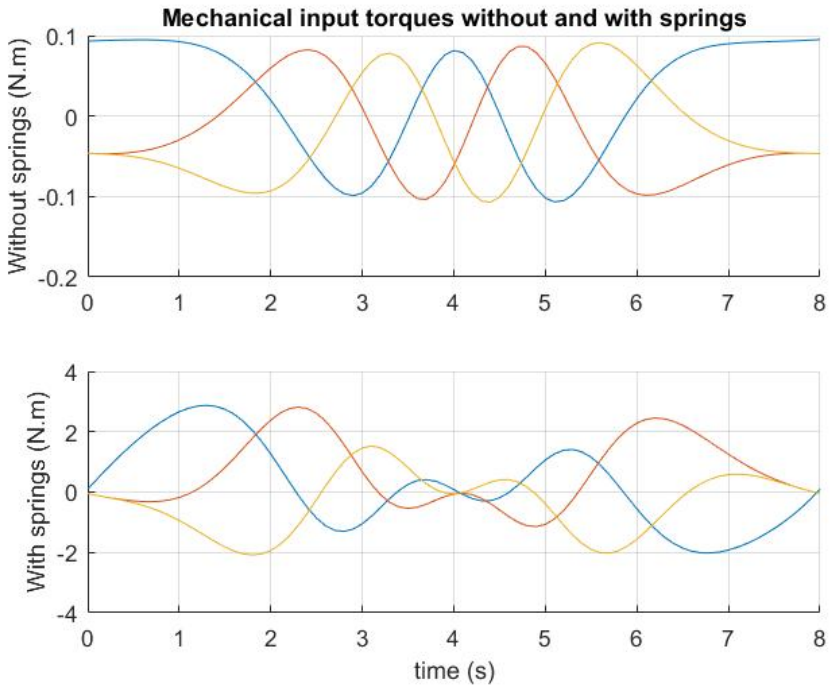

Figure 5.3: Mechanical input torque for the normal robot and with fixed stiffness springs

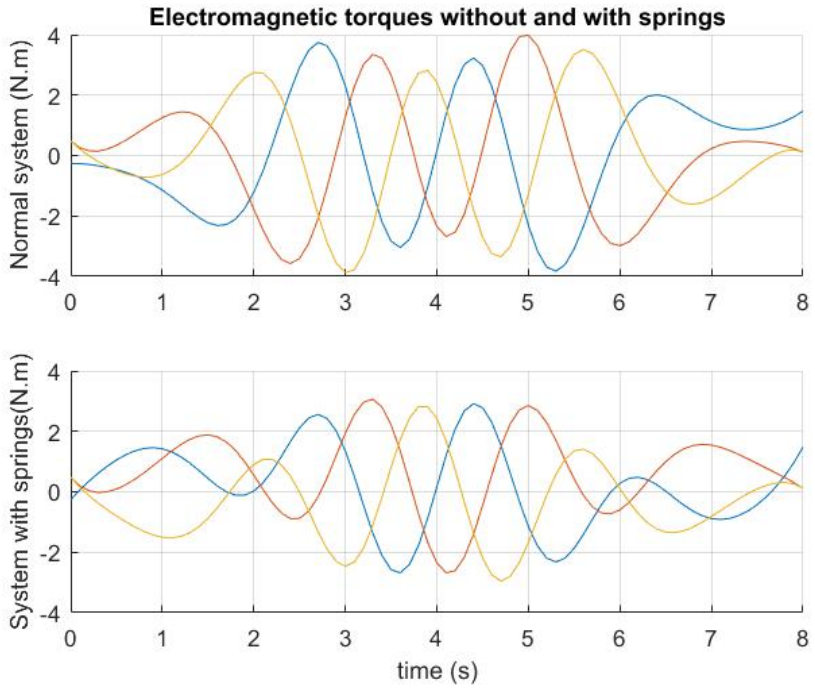

Figure 5.4: Electromagnetic torque for the normal robot and with fixed stiffness springs

5.3.2 Increase of energy efficiency

We now want to evaluate the increase of energy efficiency for a fixed stiffness system. The computation of the optimal problem based on the equation (4.28) shows that between the normal robot and the robot with fixed torsional springs in parallel with the load and the motor, the reduction of energetic losses can go up to 25%, which is already really good. These results have to be nuanced by the fact that we modeled perfect springs with no mass and no impact on the overall dynamics. We also computed the optimal spring for the test trajectory of the robot, so this stiffness could be optimal for any kind of trajectory.

The next step is to verify the reduction of energetic losses with the simulink motor model. So we run the model with the new curves of speed and torque for one given motor. The results are shown on figure 5.5.

We see that the energy efficiency is indeed improved. The gain is around 25% too, but this is nuanced by the fact that the gain computed by the optimization script takes into account the consumption of the entire robot, which means that for a given trajectory, one motor can consumes more than an other one. We see on the curves that the main amount of losses is reduced on the braking phases (around 2.5 seconds for instance). In fact at this moment, the energy is not dissipated in the motor electronics

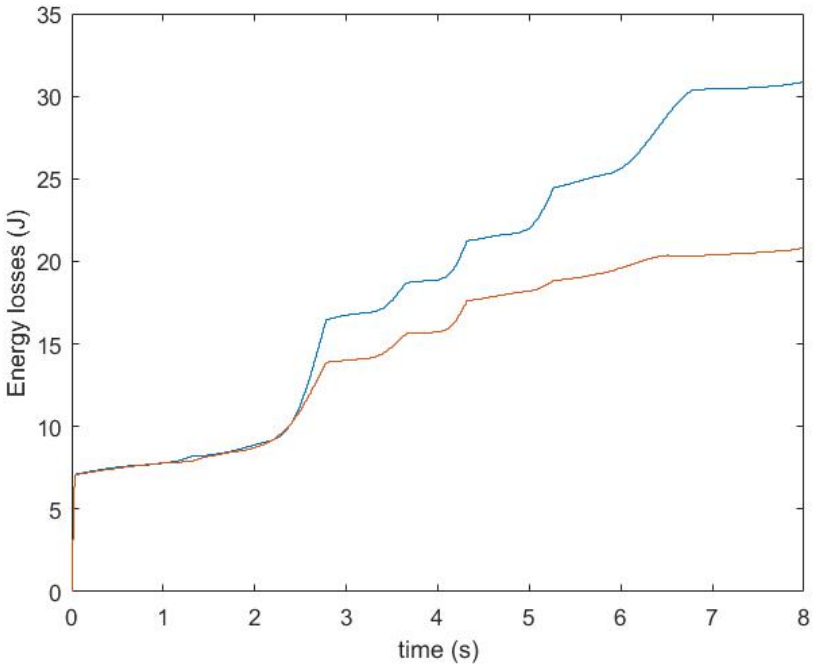

Figure 5.5: Energetic losses over the path for one motor. In blue the losses for the normal robot, in red the losses of the motor with optimal fixed stiffness

but stored in the spring, which release it afterwards. This is the effect we want to have with compliant elements, and which can be improved more with variable stiffness actuators.

5.4. Variable stiffness implementation

We now want to model the behavior of the robot and to estimate the energy consumption by using three variable stiffness actuator. Basically, the type of VSA we used is to have a VSA modifying the rest position of the spring. By doing so, we can store and restore energy at the good moment and have stiff and soft position regarding the trajectory. Several solutions to compute the evolution of stiffness have been presented in the bibliography. One can use precomputation of the stiffness, or resonance control is possible. We decided to compute the stiffness offline based on optimal theory, in order to reduce the energy consumption of the robot. The resonance control has not been studied in this master thesis.

5.4.1 Optimal problem

Once again, we reformulate the optimal problem, which is trying to reduce the energy losses of the robot. But this time, we try to optimize both the trajectory of the main motor and the VSA motor $\mathbf{q}$ and $\mathbf{q}_s$:

$$E(\mathbf{q}(\boldsymbol{\alpha}), \mathbf{q}_s(\boldsymbol{\alpha}), \alpha_k) = \int_0^T P_{losses} dt \tag{5.1}$$

With α_k the optimization variable for the fixed stiffness of the VSA. Here the losses are taking into account the losses of the ball-screw motor and the VSA motor. We first make the assumption that the VSA motor is the same than the ball-screw motor, because we already have a good model for it.

The non-linear constraints are still the respect of the dynamic model, the bounds of the trajectories and the maximal electromagnetic torques the motors can give.

5.4.2 Generation of the stiffness pattern

The main difficulty for the control and design of VSA is to find the optimal stiffness along the path. Garabini et al. [9] defined a criteria based on the first and second derivative of the position of the link :

$$\begin{cases} \sigma_{max} \text{ if } \dot{q}\ddot{q} > 0 \\ \sigma_{min} \text{ if } \dot{q}\ddot{q} < 0 \end{cases}$$

where σ is the stiffness. For a mass trajectory, based on this criteria, we can see the zones where the stiffness should be maximal and minimal (figure 5.6). The red parts show where the stiffness should be maximum in order to have the best dynamic behavior, and in blue the parts where the stiffness should be minimal. In fact, the blue parts are corresponding to the parts of the trajectory where the mass are decelerating, so the moments when we want to store energy instead of dissipate it in the motor electronics. In the same time, we want the system to be stiff on accelerating phases in order to be the most efficient.

As we do not know the exact trajectory of the VSA motor, we implemented a very permissive pattern for the trajectory including up to the third order derivative of $\mathbf{q}$ with a lot of optimization coefficients. The fixed stiffness of the VSA forming the matrix $\mathbf{K}$ is also an optimization variable.

After the running of the optimization problem, the first thing we observed is that the fixed stiffness k of the VSA computed is the same as the one we found for the fixed

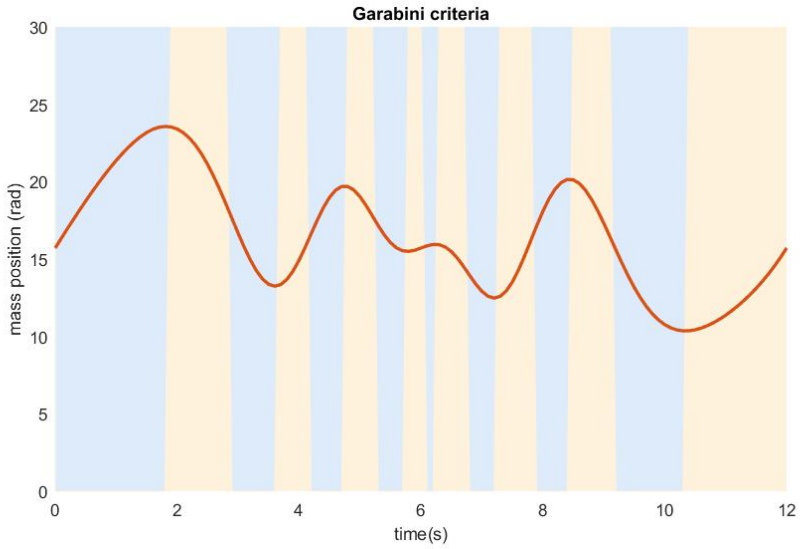

Figure 5.6: Garabini criteria applied on one mass trajectory

case. We then obtain the following trajectories for the masses and the VSA (figure 5.7). We see that the position of the VSA is not changing much, around 60°, which shows that the stiffness is softly tuned. We also computed the mechanical input torque and electromagnetic torque for all the motors (figure 5.8). We see that the values of torques for the VSA motors are less important, which means that the main part of the energetic losses are coming from the actuation of the mass.

5.4.3 Improvement of energy efficiency

We had several results for the energy losses computation. First, by taking into account the consumption of the entire robot, which means that we compute the losses due to the principal motors and the VSA motors, we obtained up to 15% of reduction of the losses. This is good but not as good as the case with the fixed stiffness. This come from the fact that for variable stiffness, our device is able to reduce energy for any kind of trajectory, whereas the fixed stiffness reduce energy only for the robot trajectory given in input of the optimal problem. VSA can be used for any robot trajectory and will reduce the losses.

If we compute the losses due to the main motor only, we achieve a reduction of energetic losses of 35%. This is good but not really representative because of course the VSA consumes energy. As we had only one model of motor, we took the same model and values for the main motor on the screw and the VSA motor. The figure 5.8 shows that the values of the torques are less important for the VSA part, so we could imagine

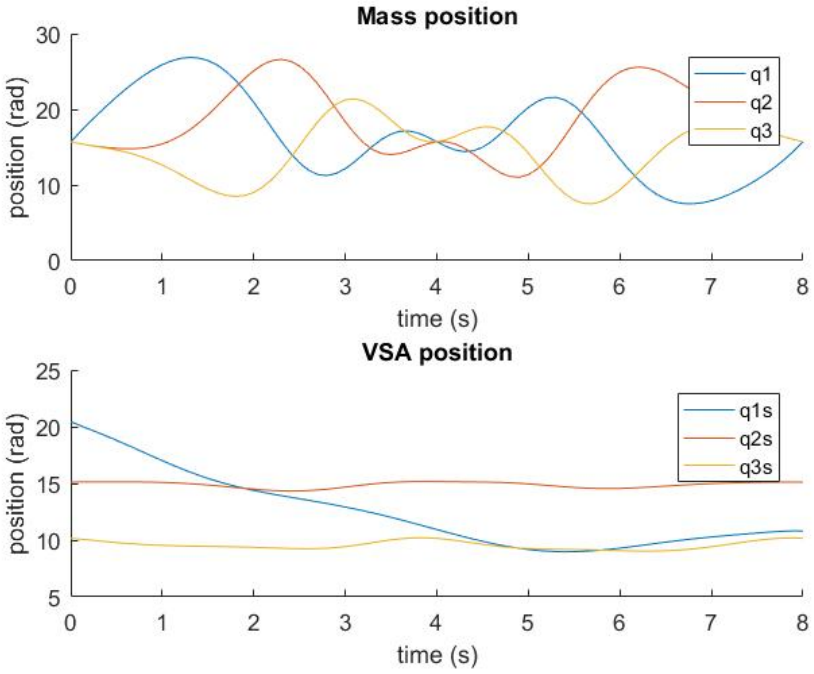

Figure 5.7: Trajectory of the masses and the VSA motor

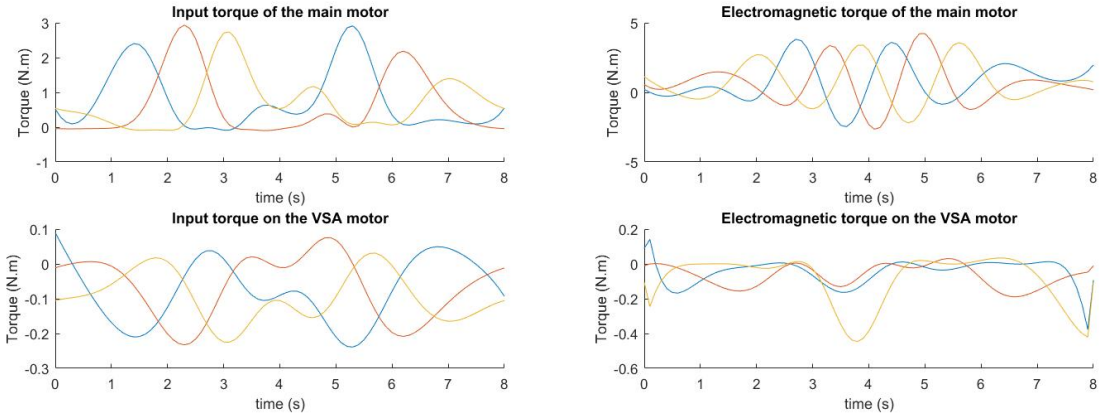

Figure 5.8: Mechanical input torque and electromagnetic torques for the mass motors and VSA motors

modify the model in order to have a way smaller motor for the VSA actuation.

A usual, in order to verify the good computation of the optimization script, we verified the results with the simulink model. We compared motor by motor the energetic losses. For one main motor, we see on figure 5.9 that the VSA permits to reduce the energetic losses more than the fixed stiffness. But the consumption of the VSA motor itself increase the overall consumption of the robot.

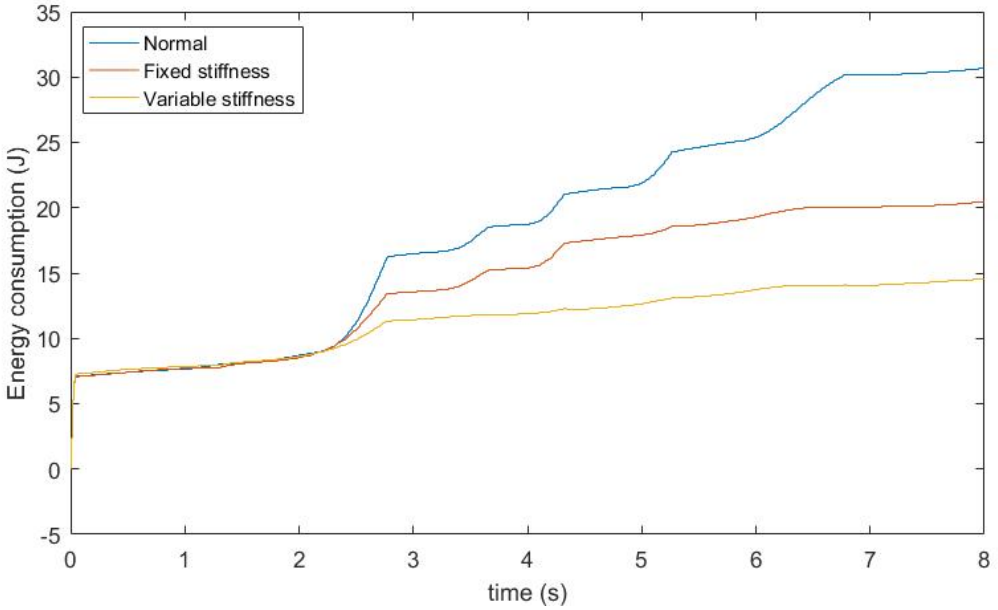

Figure 5.9: Energetic losses comparison between nominal case, fixed stiffness case and VSA case. The results are shown for one motor

5.5. Conclusion

On this section, we presented the main aspect and the main objective of this master thesis : validate the use of compliant elements for high energy efficiency in mobile robotics. We first modified the dynamic model and consumption model by including compliant elements and the consumption of the VSA motor used to tune the stiffness. Then we defined a brand new optimization problem for fixed stiffness only. We have shown that for one given robot trajectory, we can find an optimal value for the spring which reduces energy a lot. This is due to the periodic aspect of the system which works well with the springs. But for a different trajectory, we have to find a different stiffness. That is why we then used VSA in order to have a higher energy efficiency in any case. We obtained with this VSA a reduction of energetic losses up to 15%. This value could be improved by a better knowledge on the stiffness evolution. For instance, resonance control, which computes and control the VSA based on the resonance frequency of the system, could be use in order to have better results.

Chapter 6

Conclusion

6.1. Contribution of the master thesis

The aim of this master thesis was to show that compliant elements can be used for energy consumption reduction. This approach as already been made in some previous articles, only by saying that VSA improve dynamics so they increase energy efficiency. Moreover, the use of VSA for energy efficiency has never been made for mobile exploration robot, whereas it is an important field for energy efficiency, because these robots have to travel long distances with embedded batteries. This work has resonate with the work in the team focusing on energy efficiency of parallel robots, with a lot of exchange, and is a good way to prove the increase of energy efficiency for a totally different kind of system.

For this master thesis, a full and accurate model of consumption has been developed, based on a precise modeling of a brushless motor. Thus, a lot of losses have been taking into account. We also took into account the consumption of the motor used for the variable stiffness actuator, which is not made in many articles dealing with this subject.

First, we modeled a 2D cylinder rolling on a plane, actuated by three mobile masses mounted on ball-screws. For this nominal case, we computed the optimal mass trajectory, based on a energetic cost function. This cost function has been calculated thanks to an accurate modeling of the actuator and the energy losses.

On a second point, we added a fixed stiffness spring in parallel between the motor and the load. We computed the optimal stiffness of this spring for a given mass trajectory, based on the same energy consumption criteria. We have shown that we can achieve a reduction of the energetic losses of 25%. This result is nuanced by the fact that it can be achieved for one robot trajectory, and for a different one we have to modify the stiffness.

As we wanted to reduce energy consumption for all kind of trajectory, we finally modeled our robot with three VSA in place of the fixed stiffness springs. Those VSA are actuated by three independent motors, which have the same characteristics as the motors on the screw. We used once again an optimal problem in order to compute in the same time the mas trajectory and the VSA trajectory. The cost function was still the energy losses, but this time we added the losses due to the VSA motors, which are not negligible. We see that we can achieve a reduction of the losses up to 15%, whereas by not taking into account the losses in the VSA motors we have around 35% of losses reduction. 15% is not the amount of saving we expected, especially by comparing to the fixed stiffness case.

As a conclusion, this master thesis as proved that variable stiffness actuators can be used in mobile robotics in order to reduce the energy consumption of the system. The study of the losses went further with an accurate modeling of the motor, more accurate than many of the papers on the subjects.

6.2. Possible improvement and future work

This master thesis was a part of a global work about the relation between energy consumption and compliant elements. Rafael Balderas Hill (PhD student, LS2N) is working on this principle, applied to parallel robots. This work permitted to show that this principle can be used in mobile robotics. As we were working on the same aspects but on two different systems, we collaborate a lot but we also tried to experiment different techniques and fields.

The first possible improvement would be to extend the modeling of the robot to the 3D case. In fact, as the 2D model was satisfying in order to show how compliant elements can be used to increase energy efficiency, we did not go further on this point. But in order to have a real exploration robot, the modeling could be extended to a 3D case with four actuators, in order to have a fully-actuated system (possible rotation around its vertical axis).

I did not focused a lot on control aspects but more on physical modeling of the dynamic performances. That is why I mainly used optimization problems in order to obtain VSA trajectories. Meanwhile, Rafael was focusing on the control aspect of his problem and worked on the resonance control theory. The resonance control might be used for the mobile robot in order to have an efficient control and maybe improve the energy efficiency.

Rafael had also worked on a full simulink model including several motors of the

same system, exchanging energy between them in order to minimize the losses. We had no time to test it on my model, but it would be for sure very interesting, as the three motors are always non-phased. That means that when a motor is in generating mode, it could give its energy to a motor in motoring mode. By doing this, we would be able to reduce the energy losses more again.

Chapter 7

Bibliography

[1] D. Doroftei, E. Colon, and Y. Baudoin, "Development of a control architecture for the ROBUDEM outdoor mobile robot platform," no. January, 2006.

[2] R. H. Armour and J. F. V. Vincent, "Rolling in Nature and Robotics: A Review," *J. Bionic Eng.*, vol. 3, no. 4, pp. 195–208, 2006.

[3] A. H. J. A and P. Mojabi, "Introducing August: a novel strategy for an omnidirectional spherical rolling robot," *Proc. 2002 IEEE Int. Conf. Robot. Autom. (Cat. No.02CH37292)*, vol. 4, no. May, pp. 3527–3533, 2002.

[4] H. Zhuang, H. Gao, Z. Deng, L. Ding, and Z. Liu, "A review of heavy-duty legged robots," *Sci. China Technol. Sci.*, vol. 57, no. 2, pp. 298–314, 2014.

[5] A. S. Boxerbaum, J. Oro, G. Peterson, and R. D. Quinn, "The latest generation Whegs robot features a passive-compliant body joint," *2008 IEEE/RSJ Int. Conf. Intell. Robot. Syst. IROS*, pp. 1636–1641, 2008.

[6] M. Shibata, F. Saijyo, and S. Hirai, "Crawling by body deformation of tensegrity structure robots," *Proc. - IEEE Int. Conf. Robot. Autom.*, pp. 4375–4380, 2009.

[7] Y. Mei, Y.-H. Lu, Y. Hu, and C. Lee, "Energy-efficient motion planning for mobile robots," *IEEE Int. Conf. Robot. Autom. 2004. Proceedings. ICRA '04. 2004*, vol. 5, pp. 4344–4349 Vol.5, 2004.

[8] G. Lee, S. Park, D. Lee, F. C. Park, J. I. Jeong, and J. Kim, "Minimizing Energy Consumption of Parallel Mechanisms via Redundant Actuation," *IEEE/ASME Trans. Mechatronics*, vol. 20, no. 6, pp. 2805–2812, 2015.

[9] M. Garabini, A. Passaglia, F. Belo, P. Salaris, and A. Bicchi, "Optimality Principles in Stiffness Control : The VSA Hammer," no. 1, pp. 3341–3346, 2012.

[10] M. Uemura, H. Goya, and S. Kawamura, "Motion control with stiffness adaptation for torque minimization in multijoint robots," *IEEE Trans. Robot.*, vol. 30, no. 2, pp. 352–364, 2014.

[11] T. Verstraten, P. Beckerle, R. Furnémont, G. Mathijssen, B. Vanderborght, and D. Lefeber, "Series and Parallel Elastic Actuation: Impact of natural dynamics on power and energy consumption," *Mech. Mach. Theory*, vol. 102, pp. 232–246, 2016.

[12] S. Wolf, O. Eiberger, and G. Hirzinger, "The DLR FSJ: Energy based design of a variable stiffness joint," *2011 IEEE Int. Conf. Robot. Autom.*, pp. 5082–5089, 2011.

[13] B. Vanderborght, A. Albu-Schaeffer, A. Bicchi, E. Burdet, D. G. Caldwell, R. Carloni, M. Catalano, O. Eiberger, W. Friedl, G. Ganesh, M. Garabini, M. Grebenstein, G. Grioli, S. Haddadin, H. Hoppner, A. Jafari, M. Laffranchi, D. Lefeber, F. Petit, S. Stramigioli, N. Tsagarakis, M. Van Damme, R. Van Ham, L. C. Visser, and S. Wolf, "Variable impedance actuators: A review," *Rob. Auton. Syst.*, vol. 61, no. 12, pp. 1601–1614, 2013.

[14] S. Rao, R. Carloni, and S. Stramigioli, "A novel energy-efficient rotational variable stiffness actuator," *Proc. Annu. Int. Conf. IEEE Eng. Med. Biol. Soc. EMBS*, pp. 8175–8178, 2011.

[15] Y. Sugiyama, A. Shiotsu, M. Yamanaka, and S. Hirai, "Circular/spherical robots for crawling and jumping," *Proc. - IEEE Int. Conf. Robot. Autom.*, vol. 2005, no. April, pp. 3595–3600, 2005.

[16] Q. Chang-Jun, M. Pei-Sun, and Y. Qin, "A prototype micro-wheeled-robot using SMA actuator," *Sensors Actuators, A Phys.*, vol. 113, no. 1, pp. 94–99, 2004.

[17] R. Ham, T. Sugar, B. Vanderborght, K. Hollander, and D. Lefeber, "Compliant actuator designs," *IEEE Robot. Autom. Mag.*, vol. 16, no. 3, pp. 81–94, 2009.

[18] K. W. Hollander, T. G. Sugar, and D. E. Herring, "Adjustable Robotic Tendon using a Jack Spring," *Int. Conf. Rehabil. Robot.*, pp. 1–6, 2000.

[19] T. Das and R. Mukherjee, "Dynamic analysis of rectilinear motion of a self-propelling disk with unbalance masses," *J. Appl. Mech. Asme*, vol. 68, no. 1, pp. 58–66, 2001.

[20] L. Marques, a. T. D. Almeida, M. Armada, R. Fernández, H. Montes, P. González, and Y. Baudoin, "State of the Art Review on Mobile Robots and Manipulators for Humanitarian Demining," *IARP WS Humanit. Demining*, pp. 2–8, 2012.

[21] N. Ignell, N. Rasmusson, J. Matsson, S. Böttcher, R. Siegwart, I. R. Nourbakhsh, A. Seeni, B. Schäfer, and G. Hirzinger, "Introduction to Autonomous Mobile Robots," *Idt.Mdh.Se*, vol. 23, no. January, pp. 47–82, 2004.

[22] S.-M. Song and K. J. Waldron, *Machines that walk: the adaptive suspension vehicle.* MIT press, 1989.

[23] J. Bruce, K. Caluwaerts, A. Iscen, A. P. Sabelhaus, and V. Sunspiral, "Design and evolution of a modular tensegrity robot platform," *Proc. - IEEE Int. Conf. Robot. Autom.*, pp. 3483–3489, 2014.

[24] C. Germain, *Optimal Design of a two degree-of-freedom translational parallel robot for pick-and-place operations.* Theses, Ecole Centrale de Nantes, 2013.

[25] F. Pierrot, V. Nabat, O. Company, and S. Krut, "From Par4 to Adept Quattro," in *Robot. Syst. Handl. Assem. - 3rd Int. Colloq. Collab. Res. Cent. SFB 562*, (Braunschweig, Germany), pp. 207–220, Shaker Verlag, 2008.

[26] H. Goya, K. Matsusaka, M. Uemura, Y. Nishioka, and S. Kawamura, "Realization of high-energy efficient pick-and-place tasks of SCARA robots by resonance," *IEEE Int. Conf. Intell. Robot. Syst.*, pp. 2730–2735, 2012.

[27] O. Eiberger, S. Haddadin, M. Weis, A. Albu-Schäffer, and G. Hirzinger, "On joint design with intrinsic variable compliance: Derivation of the DLR QA-joint," *Proc. - IEEE Int. Conf. Robot. Autom.*, pp. 1687–1694, 2010.

[28] J. Kim, H. Yeom, F. C. P. Y. I. Park, and M. Kim, "On the Energy Efficiency of CVT-Based Mobile Robots," *Proc. Int. Conf. Robot. Autom.*, vol. 2, no. April, pp. 1539–1544, 2000.

[29] K. Hollander and T. Sugar, "Concepts for compliant actuation in wearable robotic systems," in *US-Korea Conf. CDROM*, 2004.

[30] F. Tomik, S. Nudehi, L. L. Flynn, and R. Mukherjee, "Design, fabrication and control of spherobot: A spherical mobile robot," *J. Intell. Robot. Syst. Theory Appl.*, vol. 67, no. 2, pp. 117–131, 2012.

[31] J. Giesbers, *Contact Mechanics in Msc Adams*. PhD thesis, Univerisity of Twente, 2012.

[32] H. Sagan, "Calculus of Variations and Optimal Control," *J. Franklin Insitute*, vol. 291, no. 1, pp. 991–1030, 1971.